

Photoluminescence

이정민 / 학생 / 물리·천문학부

Department of Physics and Astronomy, Seoul National University, Seoul
08826, Korea

Email : jmleeluck@snu.ac.kr

April 2023

Abstract

In this experiment, the photoluminescence effects of ruby and rhodamine 6G are observed. The temperature dependence of peak and full width half maximum(FWHM) of ruby's luminescence spectrum and that of rhodamine 6G are mainly observed. Also, the concentration of rhodamine 6G is estimated by using the FWHM of its luminescence spectrum.

1 Introduction

The main purpose of this experiment is to measure the photoluminescence signal of ruby and the solution of rhodamine 6G in ethylene glycol. To be specific, the change of photoluminescence spectra of them by varying the pressure and the temperature is mainly focused. The experiment is conducted on the atmospheric pressure and very low pressure(on average 1mTorr, and at most 10mTorr). Also, the temperature is varied from room temperature (296.7K) to 10K.

1.1 Luminescence

Some materials emit light due to the incoming energy. If the incident energy is not thermal energy, the phenomenon is called luminescence. Photoluminescence is the luminescence where the wavelength of outcoming light differs from that of the incoming light. According to the time taken for the luminescence, the photoluminescence is classified in two types: fluorescence and phosphorescence. If the substance emits the light right after the energy income, this is fluorescence. If it takes some time, this is phosphorescence.

In quantum mechanics, these phenomena are explained by the ground and excited states involved in the luminescence process. When the energy is absorbed by the materials as a form of a photon, some amount of the electrons might be excited. Since, for almost every molecule, the ground state is a singlet state, the excited state is also a singlet due to the conservation of angular momentum. The relaxation from the S_1 state, which is the lowest excited state, to the ground state S_0 state is allowed since they are singlet states. Therefore, this relaxation can occur rapidly in the 10^{-12} to 10^{-9} sec. In S_1 states and ground state S_0 , there are several vibrational modes and the excited electron is relaxed from the higher vibrational level to the lower one. Note that this process is non-radiative, but since their energy level is distinct, this results in the broadening of the wavelength of emitted photons.

However, the molecule may undergo intersystem crossing(ISC) from S_1 to excited triplet state T_1 . ISC process typically occurs when the molecule has strong spin-orbital coupling. That coupling allows the transition from singlet to triplet. The electron in the T_1 state cannot be relaxed to the ground state since their spins are distinct. This restriction is released by the spin-orbit coupling and the radiative transition from T_1 to S_1 can happen. This delayed emission process is called phosphorescence and it takes approximately from 10^{-3} to 10^5 .

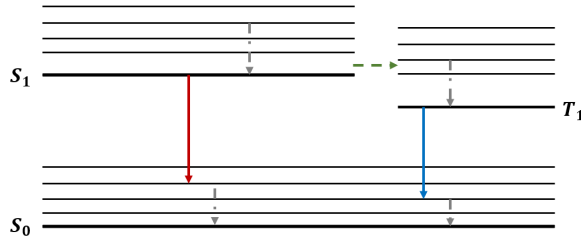


Figure 1: The diagram of photoluminescence. The thin lines refer to the vibrational modes. The red line denotes the fluorescence and the blue line denotes the phosphorescence. The dotted grey line describes the vibrational relaxaton. The dotted green line corresponds to ISC.

1.2 Ruby

1.2.1 Structure

Analyzing the molecule through the molecular orbital became a common practice in the field of natural science in the last decades. Unlike the molecules, when considering the crystal, electrons can exist on some partially continuous energy level, which is called the band. Note that this doesn't mean that electron has every energy in the crystal. There is still a region in which electrons cannot exist which is called the band gap.

Ruby is a crystal which is consisted of the aluminum ions(Al^{3+}) and the oxygen ions(O^{2-}) with chromium(Cr^{3+}) as impurities. Without the impurities, Al^{3+} sites with 6-fold oxygen have exact point groups. To be specific, Al^{3+} is an axis of C_3 group. Taking into account the tiny amount of Cr^{3+} , some Al^{3+} are replaced with the Cr^{3+} , and this results in the small distortion on the octahedral configuration.

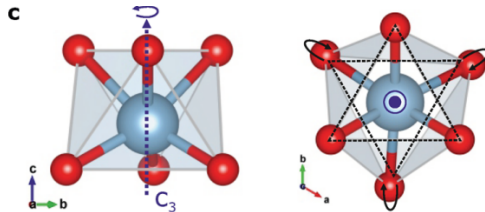


Figure 2: The symmtery of a single Al^{3+} site[1].

1.2.2 R_1, R_2 Lines

The figure 3 shows the schematization of the energy level of ruby. First of all, the optical pumping makes the electron excited on the 4T_2 and 4T_1 band. Each band's energy corresponds to green and violet light. Then, due to the strong force or the ample available phonon to carry some energy and momentum, the rapid transition $^4T_2 \rightarrow ^2T_1$ and $^4T_1 \rightarrow ^2E$ occurs. This process is nonradiative and the transition between 2E and 2T_1 isn't allowed[2]. Due to the combined action of the trigonal crystal field and spin-orbit coupling into a pair of Kramers doublets, the cubic-field state is split on the ground state 4A_2 and the first excited state 2E . The radiation from the splitted 2E to 4A_2 line corresponds to the R_1 and R_2 lines[3].

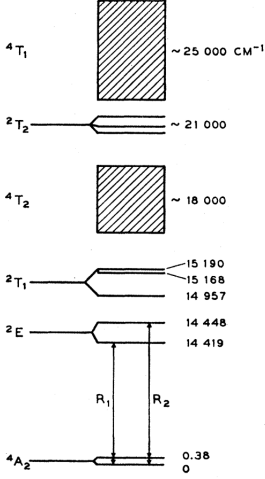


Figure 3: The lower energy level diagram of ruby.[3]

1.2.3 N-line: effect of Cr^{3+} concentration

Ruby is a crystal which is consisted of the aluminum ions(Al^{3+}) and the oxygen ions(O^{2-}) with chromium as impurities. Without the impurities, Al^{3+} sites with 6-fold oxygen have exact point groups. To be specific, Al^{3+} is an axis of C_3 group. Taking into account the tiny amount of Cr^{3+} , Al^{3+} is replaced with the Cr^{3+} ion, and this results in the small distortion on the octahedral configuration. The concentration of Cr^{3+} affects the luminescence spectra of ruby. In the previous section, only the case where the small amount of Cr^{3+} is dopped was discussed. If its concentration is sufficiently low, one can assume that the interaction between two Cr^{3+} ions is negligible. From this condition, the energy level would look like the figure 3. However, if Cr^{3+} is dopped to ruby with a nonnegligible portion, the interaction between them must be considered. That interaction appears on the spectra of a ruby as a peak due to a newly created energy level of the ruby. The extra peaks are called satellite peaks or N-lines. Note that this peak is distinct to the R lines, as the figure 4 says.

Most calculation considering the nearest neighbor of the Cr^{3+} ions cares up to the fourth nearest neighbor. Also, of all the possible radiative emission, the most significant emissions are in the figure 4. The 7009\AA line corresponds to N_1 line, while 7041\AA line is the N_2 line.

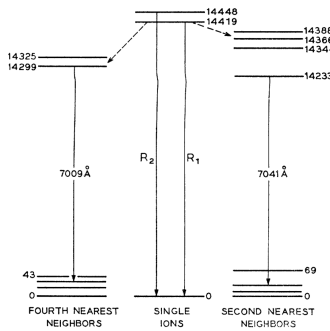


Figure 4: The energy level diagrams and N-lines of a ruby from[4]. Fine structure on the pair levels has not been shown and the values given are approximate.

The concentration dependence of the intensity ratio between the N-line and R-line is already observed and calculated. In this experiment, the doping concentration of Cr^{3+} in ruby is estimated by this relation. Moreover, the temperature dependence of the N-line is also investigated like R lines.

Relative Doping	Concentration [at.-%]	Color
Lightly Doped	< 0.1	Pink
Medium Doped	0.1 ~ 0.5	Red
Heavily Doped	> 0.5	Dark

Table 1: Atomic doping concentrations (at.-%) of Cr^{3+} and ruby color.

1.2.4 Near R-line Stokes Sideband Intensity

Around R-lines, the intensity of the Stokes sideband has been formalized first and used to identify the symmetry of the crystal. From a phonon-photon interaction, the intensity of the vibronic line increase as a fifth power of the frequency of the phonon displacement from the non-phonon line in the case where the crystal has inversion symmetry with the center ion being interested in. Without such symmetry, the intensity of the line is proportional to the cube of the phonon frequency displacement[5].

However, the precedent researches show conflicting results. For the concentration of Cr^{3+} lesser than 0.005%, the intensity becomes proportional to the cube of the phonon displacement frequency, subtracting the constant factor[6]. Without the subtraction, the intensity still follows the fifth power of the frequency[7]. In this experiment, such a relation is also observed and compared.

1.3 Rhodamine 6G

Rhodamine 6G(R6G) is the dye that is widely used for fluorescence experiments. R6G has strong absorption in the visible light region and high fluorescence yield. The molecule consists of two chromophores, xanthene, and carboxyphenyl group perpendicular to the xanthene ring[8]. This experiment uses the solution of rhodamine 6G and ethylene glycol. Ethylene glycol is one of the most widely utilized solvents of R6G. The solvent is crucial since the shape of the fluorescence spectra that this experiment primarily observes differs according to the solvent[9]. Furthermore, the concentration of R6G also affects it[10]. From this tendency, the concentration of the dye is estimated.

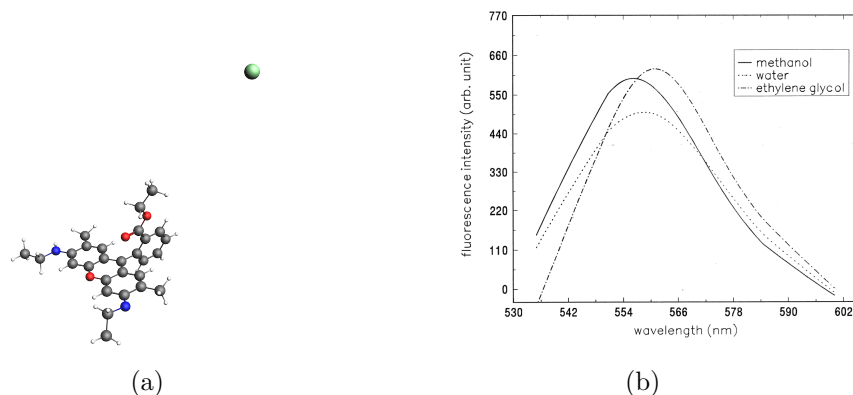


Figure 5: (a) The structure of R6G($C_{28}H_{31}ClN_2O_7$). (b) The solvent dependence of R6G fluorescence spectra. [9]

2 Method & Materials

In this experiment, the SLD-532-070T laser is used. The laser has a 532nm wavelength corresponding to the green. Also, CCD from Andor Tech. is used to convert the fluorescence signal to an electric signal. The dichroic filter is used to reflect the laser light toward the samples. In addition, it blocks the laser light reflected in the sample. Also, the notch filter is used to block some bands of light so that CCD identifies the signal from the sample more qualitatively. To conduct a low-temperature experiment, Cryostat is used. Moreover, to make the environment of very low pressure, the rotary vacuum pump is used. Finally, the vacuum gauge and temperature controller are used to read the pressure and temperature, respectively. The following figure is a diagram of the experiment setting. In figure 6, the sample denotes the rhodamine 6G or ruby. The ruby is located in the Cryostat, and rhodamine 6G is in the sealed bottle.

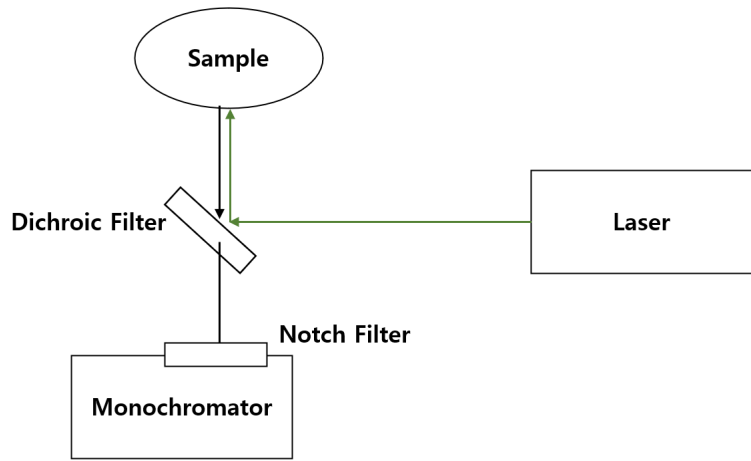


Figure 6: The simple description of experiment setting.

2.1 Rhodamin 6G Experiment

The R6G experiment is conducted at room temperature and atmospheric pressure, solely. The two types of data are collected: background and reference. The reference data is a signal whose background is removed. The data is collected with the central wavelength of 567nm and 590nm. The reason for measuring the data with a central wavelength of 590nm is to observe the anti-symmetric property of the spectra.

2.2 Ruby Experiment

On the contrary, for the ruby, the experiment is conducted in several temperatures including a room temperature of 296.7K. Also, the shape of ruby spectra in very low pressure and atmospheric pressure is observed. To be specific, the temperature is set up from 10K to 280K at the interval of 10K. In addition, almost every low-pressure experiment is conducted on 1mTorr, but some experiment is approximately 10mTorr. The data is gathered with a central wavelength of 700nm. Like the R6G experiment, background data and reference data are collected.

3 Experiment & Result

3.1 Rhodamine 6G

The figure 7 shows the fluorescent spectra of R6G at room temperature. The fitting model is the linear combination of two gaussian functions : $a_1 \exp(-[(x - b_1)/c_1]^2) + a_2 \exp(-[(x - b_2)/c_2]^2)$. Since the spectra seems that it has two peaks, the linear combination of two gaussian functions is used rather than a single gaussian.

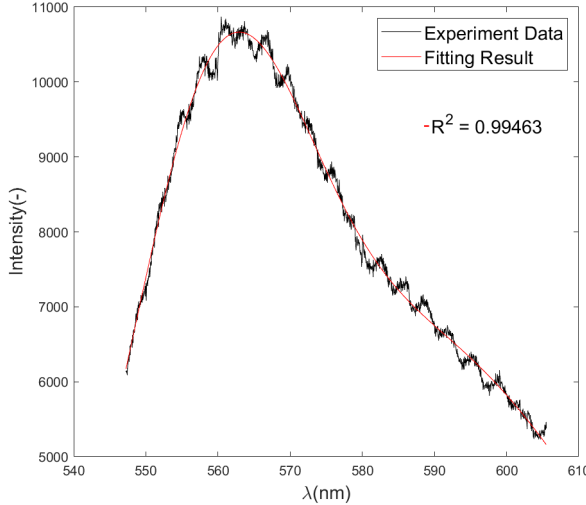


Figure 7: The experiment data and fitting result of R6G fluorescent spectra.

Coefficient Name	Coefficient	2σ error
a_1	6486.694900	773.8894
b_1	559.538410	0.2594
c_1	17.263039	0.757543
a_2	6502.612700	162.1869
b_2	586.891220	2.41784
c_2	38.617666	3.245692

Table 2: The coefficient and 2σ error of gaussian fitting.

The peak wavelength and the full width half maximum(FWHM) are estimated based on the result of fitting and 2σ confidence interval. See the supplementary materials to check the calculation of FWHM, peak wavelength and their error.

	Estimated Value	2σ error
FWHM[nm]	58.8059	1.2451
Peak Wavelength[nm]	562.9313	0.36

Table 3: The estimated peak wavelength and FWHM of R6G fluorescent spectra with 2σ error.

3.2 Ruby

3.2.1 Pseudo Voigt Profile

Unlike the proposition from [11], some data in ruby analysis are fitted by using Pseudo-Voigt profile to analyze the data and their errors more thoroughly. The pseudo-Voigt functions are defined as the following adopted from [12].

$$\phi_l(\nu) = 2A_l \left[\frac{G}{W_l} \sqrt{\frac{\ln 2}{\pi}} \exp \left\{ -4\ln 2 \left(\frac{\nu - C_l}{W_l} \right)^2 \right\} + \frac{L}{\pi \left[1 + \left(\frac{\nu - C_l}{W_l} \right)^2 \right]} \right] \quad (1)$$

with A_l the area, G_l the Gaussian shape factor (the Lorentzian shape factor $L = 1 - G$), W_l is the FWHM, and C_l is the center (peak position) of each the spectral each for the corresponding peak number l . The total multiple Voigt profile is the sum of multiple single Voigt profiles.

$$\Phi(\epsilon) = \sum_{l=1}^{15} \phi_l(\epsilon) \quad (2)$$

3.2.2 R_1, R_2 Lines

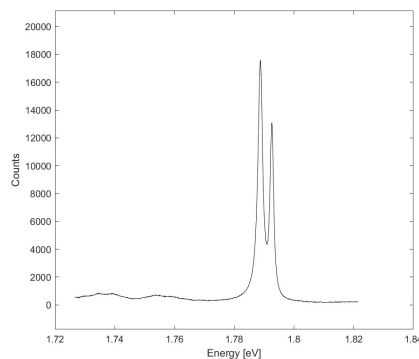


Figure 8: Experimental result of Ruby spectrum on 296.7K, 1atm. Wavelength domain is converted into eV unit.

As one can see in the figure above, the luminescence spectra from the ruby sample have significant double peaks which correspond to R_1 and R_2 lines. The following figures show the result of fitting to analyze the peak position and the width. Likewise, the other figures are in the supplementary materials.

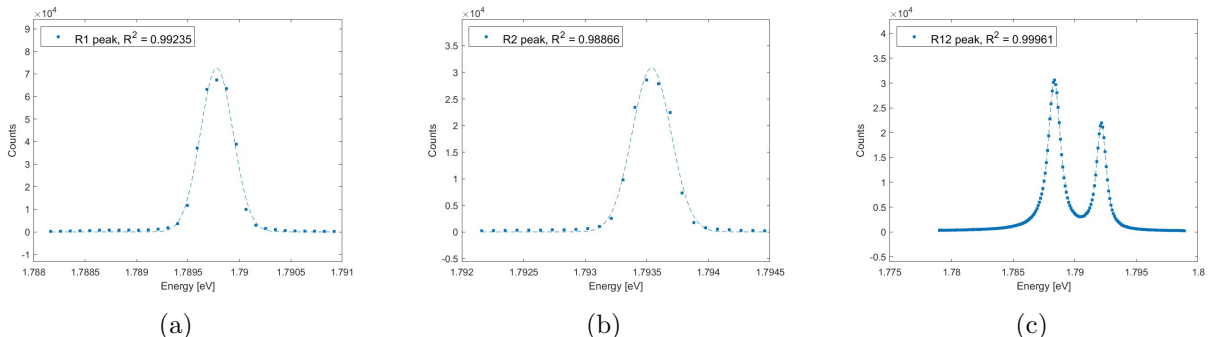


Figure 9: (a), (b) Fitting of each R_1, R_2 peaks of 70K, 10mTorr by pseudo-Voigt function. (c) Fitting of peaks of 296.7K, 1atm using binomial voigt function.

Due to the effect of peak broadening, the Voigt profile is used to fitting the experiment result[11]. The Gaussian function represents the superposition of a range of spectral lines which have various central wavelengths. The discordance of the central wavelength is due to each line having a certain environment at the instant of the transition. Moreover, the Lorentzian function represents the collision between the atoms[13].

For a high temperature, the bimodal Voight fitting is conducted. In contrast, for relatively low temperatures ($T < 80\text{K}$), pseudo-Voight fitting is performed. From this analysis, one can get the peak position, its height, and FWHM.

Thermal line shift of peak energy, that is the position of peak energy domain comes from the absorption and re-emission of phonon[13]. Hamiltonian of lattice-ion interaction can derive this value. The equation 3 shows the result of the calculation of the Hamiltonian[13]. Under the specific condition($\Delta E \gg \hbar\omega_D$), which holds as the Debye temperature $T_D < 1000\text{K}$, the terms that represent perturbation between ion and phonon are negligible. Since the Debye temperature of ruby is, in general, 760K, the last two terms of eqaution 3 are negligible.

$$x = x_0 + \alpha \left(\frac{T}{T_D} \right)^4 \int_0^{T_D/T} \frac{x^3}{e^x - 1} dx \\ + \sum_{j < i} \beta_{ij}^n \frac{T}{\Delta E_{ij}} P \int_0^{T_D/T} \frac{x^3}{e^x - 1} \frac{1}{x^2 - (\Delta E_{ij}/KT)^2} dx \\ - \sum_{j > i} \beta_{ij}'' \left(\frac{T}{\Delta E_{ij}} \right)^2 P \int_0^{T_D/T} \frac{x^3}{e^x - 1} \frac{1}{x^2 - (\Delta E_{ij}/KT)^2} dx \quad (3)$$

The following figure shows the position of R_1 , R_2 line on luminescence spectra in several temperatures. One can see that the fitting result accords with the experiment results. The coefficients used in the fitting are given in the table 4.

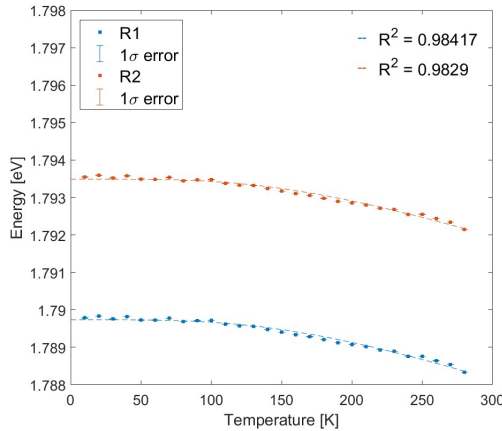


Figure 10: Experimental result and fitting result of peak shift of R_1 , R_2 lines.

Line	α	ϵ_0
R_1	$-0.0347 \pm 8.624 \times 10^{-4}$	$1.790 \pm 1.483 \times 10^{-5}$
R_2	$-0.0334 \pm 8.653 \times 10^{-4}$	$1.7935 \pm 1.488 \times 10^{-5}$

Table 4: The fitting coefficients of thermal shift of R lines based on equation 3 with 1σ stand error.

The interaction between the phonons can also affect thermal broadening. Several effects such as the uncertainty principle, or Doppler effect must be considered for FWHM. Due to the relaxation of phonon, some factors are possible to quantization under the temperature-differing condition[13].

$$\begin{aligned} \Gamma = & \Gamma_0 + \beta \left(\frac{T}{T_D} \right)^7 \int_0^{T_D/T} \frac{x^6 e^x}{(e^x - 1)^2} dx \\ & + \sum_{f>i} \beta_{if} \frac{1}{e^{\hbar\omega_{fi}/KT} - 1} + \sum_{f< i} \beta_{if} \frac{e^{\hbar\omega_{if}/KT}}{e^{\hbar\omega_{if}/KT} - 1} \end{aligned} \quad (4)$$

While excluding the relaxation between two phonons (Orbach process), the last two terms of equation 4 are negligible. The following figure shows the result of fitting from the FWHM of spectral lines As the peak position fitting, the results of figure 11 agree with the experimental data. The fitting coefficients are listed in the table 5.

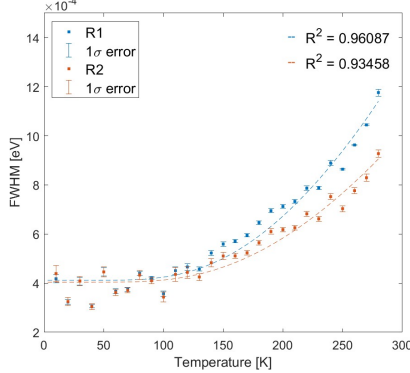


Figure 11: Experimental result and fitting result of peak fwhm of R_1 , R_2 lines.

Line	β	v_0
R_1	$4.14 \times 10^{-4} \pm 1.160 \times 10^{-5}$	0.0406 ± 0.0016
R_2	$4.037 \times 10^{-4} \pm 1.047 \times 10^{-5}$	0.0279 ± 0.0014

Table 5: The fitting coefficients of thermal broadening of R lines based on equation 4 with 1σ stand error.

As the heat interaction between the initial state of R_1 , R_2 lines obeys the Boltzman statistic, the frequency which is propotional to each peak intensity would have ratio as eqaution 5.

$$\frac{I_2}{I_1} = A e^{-\Delta E/k_B T} \quad (5)$$

where ΔE denotes photon energy difference of R_1 , R_2 , and k_B is Boltzman constant. To conduct the linear fitting, we take a logartithm on both side of eqaution 5.

$$\log \left(\frac{I_2}{I_1} \right) = -\frac{\Delta E}{k_B T} + \log(A) \quad (6)$$

The following figure is the result of the fitting based on the equation 6. For the fitting below, the assumption that ΔE is invariant about the temperature is introduced. From the figure 12, ΔE and the intercept A are calculated and listed in the table 6.

$\Delta E[eV]$	A
$0.00279 \pm 5.02 \times 10^{-5}$	0.6575 ± 0.0092

Table 6: The estimated value of ΔE and A with 1σ stand error.

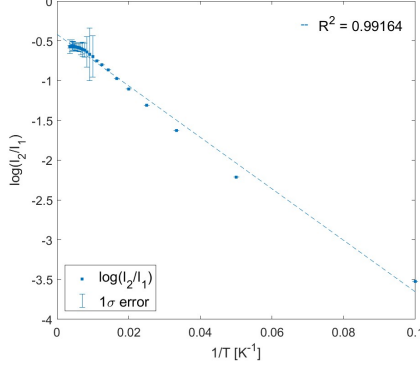


Figure 12: Experimental result and fitting result of peak intensity ratio of R_1 , R_2 lines. log fitting about $1/T$ is performed to observe liner depndency.

In fact, the temperature-averaged ΔE obtained from the peak position and its width is $0.00377 \pm 1.596 \times 10^{-5}$. Even though the value is underestimated, the fitted ΔE has similar magnitude of order with experimental ΔE .

4 Discussion

4.1 N1-line

The tiny peak at $1.7698eV$ is identified as the N_1 line whose wavelength is 7009\AA ($1.7689eV$). Note that N_2 line is not resolvable. The baseline of the N_1 line is removed using a 3rd order polynomial fit, and the peak is fitted with the Gaussian profile of the temperature from 10K to 230K. To get resonable error analysis and compute rapidly, the Gaussian profile is used rather than a Voight profile. See supplementary materials to get the results of N-line fitting and its coefficients with the error.

4.1.1 Temperature Dependent Shift and FWHM of the N1-line

The results were fitted with equation 3 and 4, with the Debye temperature as $T_D = 760\text{K}$ [14].

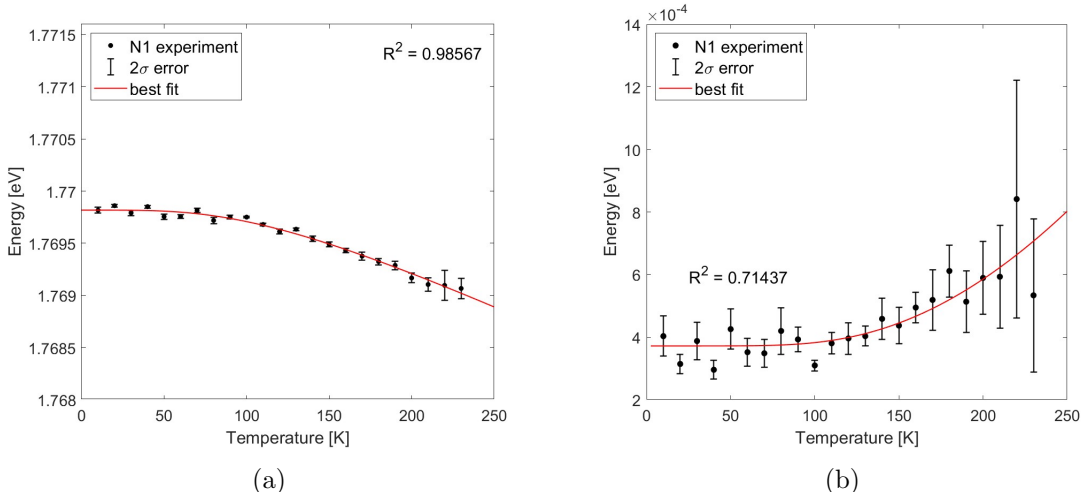


Figure 13: (a) The experiment data and fitting result of the peak position of the N_1 line. (b) The experiment data and fitting result of the FWHM of the N_1 line

Type	Scale Factor	Intercept
Peak Wavelength	-0.0327 ± 0.0012	$1.7698 \pm 1.31 \times 10^{-5}$
FHWM	$3.31 \pm 0.46 \times 10^{-2}$	$3.72 \pm 0.18 \times 10^{-4}$

Table 7: The fitting coefficients of thermal shift of N_1 line with 1σ stand error. Note that scale factor denotes α for equation 3 and β for equation 4. Also, the intercept is x_0 for equation 3 and ϵ_0 for equation 4

4.2 Stokes Sideband

4.2.1 Near R-line Stokes Sideband Intensity

Since the counts of the Stokes sideband near the R-line($1.7617\text{eV} \sim 1.778\text{ eV}$) refer to the intensity, they are used for the intensity measurement. A constant bias of the average intensity for energy from 1.78eV to 1.785eV is subtracted. This region has the lowest energy values between the R-line and the Stokes sideband. The visible N_1 line is also removed for this analysis.

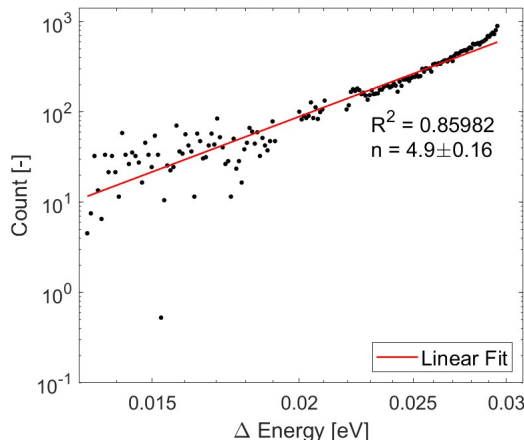


Figure 14: The experiment data and linear fit of the intensity and the energy of the Stokes sideband phonon frequency displacement from the R1-line.

The results were linearly fitted in a log-log plot, and the slope results to be $n = 4.9 \pm 0.16$. From the previous research, this result implies that the ruby has sufficient inversion symmetry. The reason that a slightly lower value came out is due to the imperfect inversion symmetry in ruby. Even though perfect inversion symmetry is unlikable, the figure 14 says that the octahedral symmetry is only slightly distorted[7].

4.2.2 Sideband Fitting

A fitting for the Stokes sideband is also tried. In the begining, a genetic algorithm is used to converge the fit rapidly. Then, the result of the algorithm is tuned by using the nonlinear fitting tool in MATLAB. The nonlinear fitting is conducted by the Pseudo-Voigt profile. The initial estimation of the peak values was already taken[7].

$$\omega = \left[\frac{\sum_{\epsilon_i} (y_i - \Phi(\epsilon_i))^2}{\sum_{\epsilon_i} (y_i - \overline{\Phi(\epsilon_i)})^2} \right] \quad (7)$$

The fitting results, however, were not sufficient to analyze the properties of each peak. The background data of figure 15 cannot be separated and this probably makes some distortion of

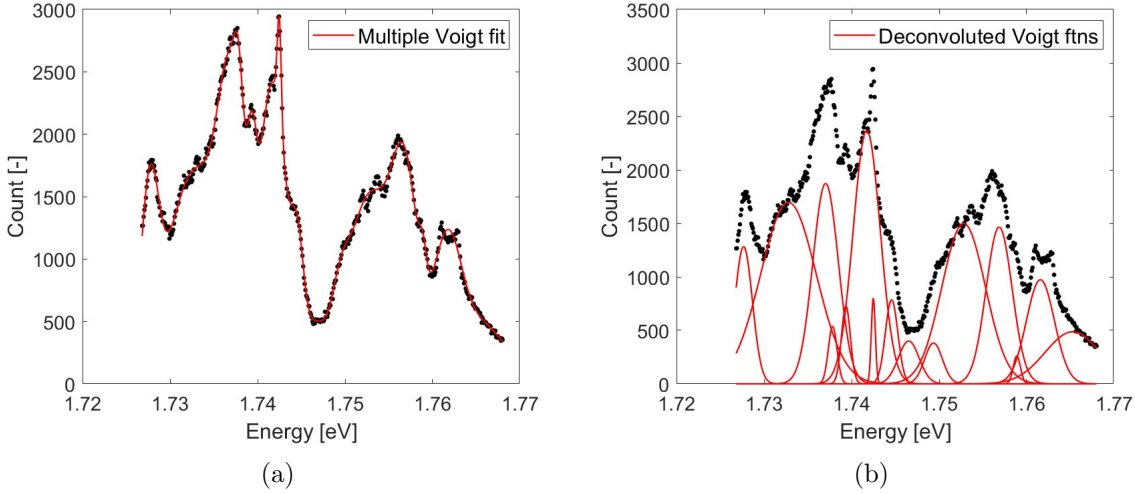


Figure 15: (a) The Stokes Sideband of the fluorescence spectrum and the fitted result. $R^2 = 0.9952$ (b) The decomposed Voigt functions

the fitting. Therefore, this method has an essential limitation and to explain the shape of Stokes sideband properly, one has to re-design the total experiment. However, in this experiment, it is not a main purpose, so leave it as a follow-up study.

4.3 Pressure Dependence of R lines

In room temperature of 296.7K, the spectra of ruby is obseved with the pressure of 9.1mTorr and 763Torr, which is 1atm.

Line	position	FWHM
R_1 , 1atm	$1.7873 \pm 2.322 \times 10^{-6}$	$5.70 \times 10^{-5} \pm 3.72 \times 10^{-7}$
R_2 , 1atm	$1.7912 \pm 2.781 \times 10^{-6}$	$3.25 \times 10^{-4} \pm 1.20 \times 10^{-5}$
R_1 , 9.1mTorr	$1.7873 \pm 2.193 \times 10^{-6}$	$5.70 \times 10^{-5} \pm 3.53 \times 10^{-7}$
R_2 , 9.1mTorr	$1.7912 \pm 2.686 \times 10^{-6}$	$3.53 \times 10^{-4} \pm 1.13 \times 10^{-5}$

Table 8: Fitting Result of R_1, R_2 peak's position and fwhm varying pressure.

From table 8, it seems there are no dependence of peak position or broadening. This is because the pressure near atmospheric pressure is not big enough to give any difference of optical properties. Ruby's peak position is proportional to $1/\rho^2 v^{10}$ and peak broadening is proportional to $1/\rho v^5$ where ρ is density and v is phonon speed, and they are dependent about temperature. Since ruby's stiff modulus is order of $1.3 \pm 0.03 \times 10^{-4}$ [kbar $^{-1}$], atmospheric pressure compress ruby in a factor of 1.3×10^{-7} , which is too small to change density, velocity, or other lattice properties[15]. In fact, other researchs which try to find the relation between the pressure and the crystal studied in GPa unit, which is much bigger than our magnitude [16].

4.4 Ripples on R6G Luminescence Spectra

In figure 7, one can see the periodicity of intensity. To see the periodicity more clearly, the fast Fourier transform is conducted. To remove the effect of the noise, data is smoothed. Then, from the smoothed data, the ripple is seperated by subtracting the fitting result. Note that the

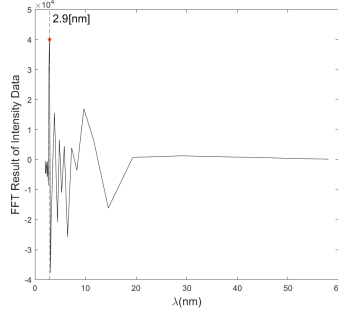


Figure 16: FFT of the ripple on the fluorescent spectra of R6G.

fitting result regards the trend of the spectra. From figure 16, the periodicity of the spectra is explicit.

We conclude that this phenomenon is due to the fallacies of the experimental instruments. One may maintain that the ripples are the result of Resonance Raman scattering. However, the Raman shift of R6G does not accord with the wavelength where the ripples occur. Furthermore, due to the strong fluorescent effect, in Raman spectroscopy, the wavelength of the optical pumping is set to approximately 480nm[8]. Otherwise, the strong fluorescent light might swallow the small peaks caused by the resonance between the laser and the electronic transition of R6G. Therefore, the consideration of Resonance Raman scattering is meaningless. In addition, several experiments observed the fluorescent spectra of R6G in ethylene glycol without the ripples[9, 10, 17]. In this respect, the fallacies of the experimental instruments are highly suspected. The possible flaws are the failure to align the monochromator or the laser, the degradation of electronic devices, or the problem with the R6G solution.

4.5 Dimer Effect of R6G

In figure 7, the linear combination of the Gaussian function was used for the fitting due to the dual peaks on the fluorescent spectra. This is the effect of the dimer[18]. The dimer spectrum has two visibly separated bands like the figure 17 (b) [10]. The reason for dual peaks on pure dimer fluorescent spectra is that, unlike monomer, dimer has two split energy level : E_H & E_J in figure 17 (a).

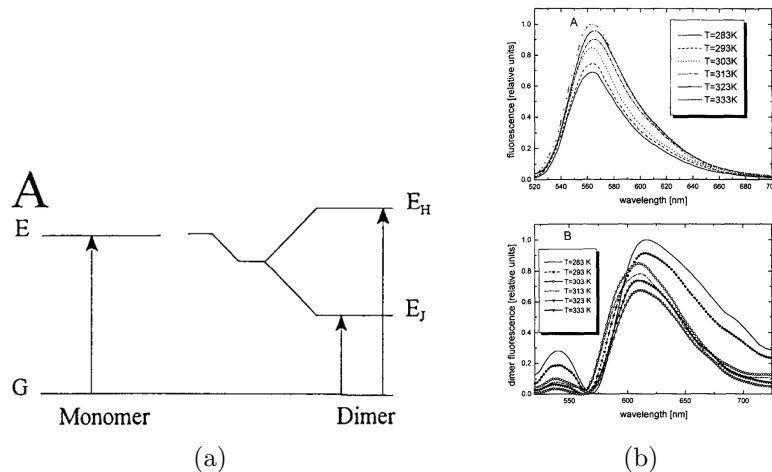


Figure 17: (a) Electronic energy diagram[10]. (b) The observed spectra of monomer and dimer from [10] : upper one is the monomer fluorescent spectra and lower on is the dimer fluorescent spectra.

To evaluate how strongly the dimer affects the total fluorescent spectra in this experiment, the quantum yield, or the temperature dependence of the spectra must be observed. For the case where the dimer effect is meaningful, the peak intensity decreases as the temperature rises[10]. Thus, for further investigation, additional experiments are necessary: for instance, the data for absorption spectra, or the variation of fluorescent spectra by varying the temperature.

4.6 Concentration Estimation

4.6.1 Rhodamine 6G

In this experiment, the ethylene glycol is used as a solvent. From the relation between the concentration of R6G and the peak wavelength, the concentration of R6G used in this experiment can be calculated. First of all, the concentration of R6G can be expected from the figure 18. Comparing the color of the solutions, the concentration of R6G is expected to be $100\mu M$.

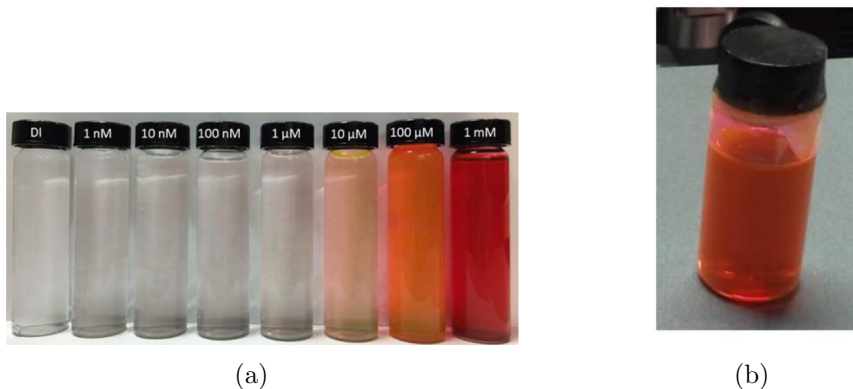


Figure 18: (a) The color of solution varying the concentration of R6G[19]. (b) the real sample of R6G in this experiment[11].

To analyze more precisely, the concentration estimation based on the peak wavelength is performed. The relation between the concentration and the peak wavelength is already calculated. However, the given reference does not provide the raw data, we interpolate the data on figure 19 by using Tracker. See supplementary materials to get the information of interpolation process. As a result, the concentration of R6G is $125.23 \pm 41.11\mu M$ with 2σ error. One can notice that the estimation quite agrees with the expectation by eye, above.

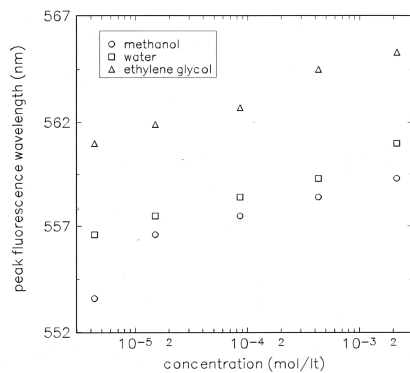


Figure 19: The calculated relation between peak wavelength and concentration of R6G.[9]

4.6.2 Ruby

As the relation between the Cr^{3+} concentration and the intensity ratio of N_1 and R_1 mentioned above, the estimation for doping is possible. Considering the reason for appearance of N_1 line, the intensity of it increases for higher doped sample. However, a theoretical model for it have not been investigated precisely due to the limitation such as a non-uniformly doped Ruby.

Therefore, to expect the concentration of Cr^{3+} , the experiment conducted on [4] are referred. From the figure 3 in [4], linear regression is performed to allow some estimations of the Cr^{3+} doping at specific intensity ratio. The figure 20 (a) below shows the result of linear regression. Since the experiment of [4] is conducted on 77K, the intensity ratio of two lines is plotted and fitted with 3rd order polynomial. The figure 20 (b) shows the result. The error when using the values from figure 3 of [4] is estimated to be 3%. The abnormal increment of the error bar in figure 20 (b) is due to the variation of fitting profile.(from pseudo-Voigt to Voigt¹) All successive error in the fits were considered in the result. See supplementary to get the coefficients of the fitting and the error, below.

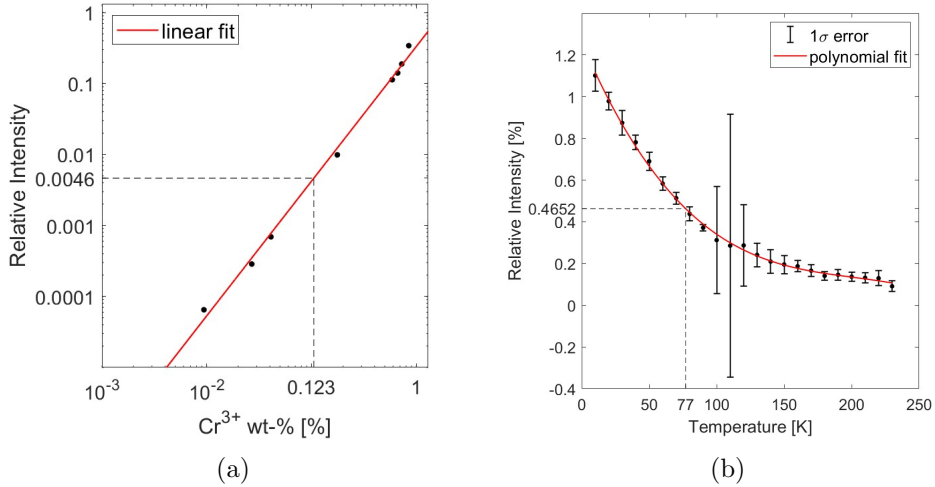


Figure 20: (a) The R-line N-line intensity ratio given by Fig 3. of [4] with a linear fit ($R^2 = 0.9958$). (b) The R-line N-line intensity ratio by temperature with a 3rd order polynomial fit ($R^2 = 0.9942$).

As a result, the concentration of Cr^{3+} is estimated 0.0650 ± 0.004 wt.-% and 0.0348 ± 0.0023 at.-%. This implies that the ruby is lightly doped and from the table 1, the color of ruby should be pink. One can find that the color of ruby used in this experiment is also pink from the figure 21. The possible error of this estimation can occur when calculating the intensity ratio. The reference data used here is calculated from the sum of all polarization. However, in this experiment, it is impossible to change the polarization of the laser. In this respect, the proposition might be not that accurate.

¹The Voigt fitting gave incompetently large error for single peak fitting results.

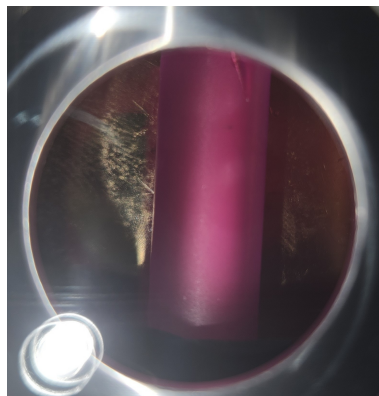


Figure 21: The ruby used.

References

- [1] Myrtille O.J.Y Hunault, Yoshihisa Harada, Jun Miyawaki, Jian Wang, Andries Meijerink, Frank M. F de Groot, and Matti M van Schooneveld. Direct observation of Cr^{3+} 3d states in ruby: Toward experimental mechanistic evidence of metal chemistry. *The journal of physical chemistry. A, Molecules, spectroscopy, kinetics, environment, & general theory*, 122(18):4399–4413, 2018.
- [2] Joseph A. Calviello, Edward W. Fisher, and Zindel H. Heller. Direct $2\pi 1/2$ e phonon relaxation in ruby and its effect upon r-line breadth. *Journal of applied physics*, 37(8):3156–3160, 1966.
- [3] D. F. Nelson and M. D. Sturge. Relation between absorption and emission in the region of the r lines of ruby. *Physical review*, 137(4A):A1117–A1130, 1965.
- [4] A. Monteil and E. Duval. Energy transfer in ruby. *Journal of luminescence*, 18:793–796, 1979.
- [5] Lawrence A. Vredevoe. Low-temperature electric dipole vibronic transitions in rocksalt- and zinc-blende-type structures. *Phys. Rev.*, 147:541–544, Jul 1966.
- [6] S. E. Stokowski, S. A. Johnson, and P. L. Scott. Vibronic transitions in ruby and $\text{MgO}:V^{2+}$. *Phys. Rev.*, 147:544–546, Jul 1966.
- [7] U. Rothamel, J. Heber, and W. Grill. Vibronic sidebands in ruby. *Zeitschrift f r Physik B Condensed Matter*, 50(4):297–304, 1983.
- [8] Lasse Jensen and George C Schatz. Resonance raman scattering of rhodamine 6g as calculated using time-dependent density functional theory. *The journal of physical chemistry. A, Molecules, spectroscopy, kinetics, environment, & general theory*, 110(18):5973–5977, 2006.
- [9] C. BINDHU, S. Harilal, V P N Nampoori, and C. VALLABHAN. Solvent effect on absolute fluorescence quantum yield of rhodamine 6g determined using transient thermal lens technique. *Modern Physics Letters B*, 10:563–576, 07 1999.
- [10] P. Bojarski, A. Matczuk, C. Bojarski, A. Kawski, B. Kukliński, G. Zurkowska, and H. Diehl. Fluorescent dimers of rhodamine 6g in concentrated ethylene glycol solution. *Chemical physics*, 210(3):485–499, 1996.

- [11] Min Young Kim. *Photoluminescence*. Department of Physics and Astronomy, SNU, 2023.
- [12] Seetha Raghavan, P.K Imbrie, and William A Crossley. Spectral analysis of r-lines and vibronic sidebands in the emission spectrum of ruby using genetic algorithms. *Applied spectroscopy*, 62(7):759–765, 2008.
- [13] RICHARD CONGER POWELL. The interaction of chromium ions in ruby crystals, 1967.
- [14] Richard C. Powell, Baldassare DiBartolo, Behzad Birang, and Charles S. Naiman. Temperature dependence of the widths and positions of the r and n lines in heavily doped ruby. *Journal of applied physics*, 37(13):4973–4978, 1966.
- [15] Larry W. Finger and Robert M. Hazen. Crystal structure and compression of ruby to 46 kbar. *Journal of applied physics*, 49(12):5823–5826, 1978.
- [16] Kazutaka Nakano, Yuichi Akahama, Yasuo Ohishi, and Haruki Kawamura. Ruby scale at low temperatures calibrated by the nacl gauge: Wavelength shift of ruby r1 fluorescence line at high pressure and low temperature. *Japanese Journal of Applied Physics*, 39(Part 1, No. 3A):1249–1251, 2000.
- [17] Ma Heupel, I Gregor, St Becker, and E Thiel. Photophysical and photochemical properties of electronically excited fluorescent dyes: a new type of time-resolved laser-scanning spectroscopy. *International journal of photoenergy*, 1(3):165–172, 1999.
- [18] I T Sugiarto, Isnaeni, and K Y Putri. Analysis of dual peak emission from rhodamine 6g organic dyes using photoluminescence. *Journal of physics. Conference series*, 817(1):12047, 2017.
- [19] Hsuan-Chao Hou, Yaser Banad, and Safura Sharifi. Detection of complex molecular samples by low-cost surface enhanced raman spectroscopy (sers) substrate. page 101671P, 04 2017.

Supplementary Materials : Photoluminescence

Jeong Min Lee

Department of Physics and Astronomy, Seoul National University, Seoul
08826, Korea

Email : jmleeluck@snu.ac.kr

June 1, 2023

S1 Rhodamin 6G

S1.1 Peak Wavelength & FWHM Calculation

Since there is no explicit form of the maximum value's location in the linear combination of the gaussian function, the error of peak wavelength and FWHM are calculated based on the 1σ confidence interval. Each confidence interval of b_1, b_2 is related to the location of the maximum value. Both sides of the interval show the possible rightmost spectra and leftmost spectra. From this observation, the error of peak wavelength in the fitting can be regarded as a peak wavelength of them. Likewise, each confidence interval of c_1, c_2 is related to the width of the spectra. They may show the possible narrow spectra and broad spectra. They are also regarded as the error of FWHM of the fitted spectra in this experiment.

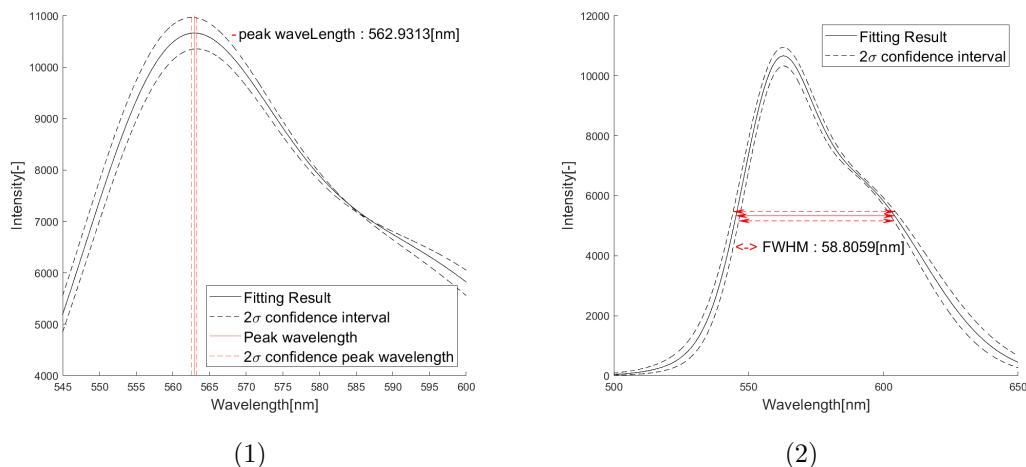


Figure S1: (a) The peak wavelength with rightmost and leftmost one. (b) The FWHM with narrow and broad one.

S1.2 Interpolation by Tracker

Since we cannot get the raw data of the figure below, interpolation by using Tracker is our best to estimate the most reliable concentration. We provide the uncertainty of the ruler tool on the Tracker and the error of peak wavelength as an error of this estimation. The following figure shows a single example of the process of interpolation.

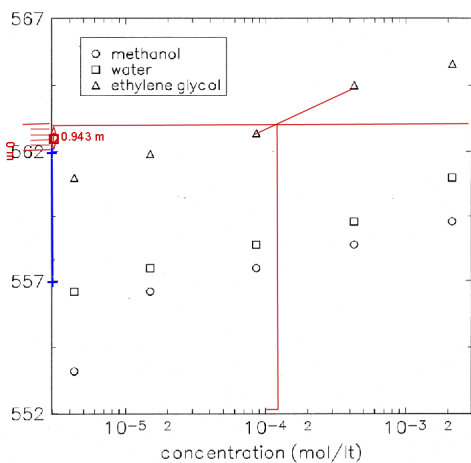


Figure S2: The interpolation on the relation between the concentration of R6G and peak wavelength by using Tracker.

S2 Ruby Sideband Fitting Results

peak Num	Total Area	Gaussian Factor	FWHM	Peak Position
1	3.715509	0.871601	0.002372	1.727664
2	11.58015	1.162326	0.007452	1.732788
3	5.911396	1.163725	0.003448	1.737033
4	2.178878	0.307087	0.00117	1.737838
5	1.589836	0.590564	0.001214	1.739351
6	2.118599	0.563544	0.002802	1.746523
7	4.448429	2.066574	0.003644	1.741731
8	1.064338	0.435615	0.000544	1.742481
9	3.078287	0.458258	0.001686	1.744572
10	1.118812	0.869593	0.002395	1.749358
11	1.134881	0.238084	0.000974	1.758876
12	6.818242	1.37069	0.005851	1.752803
13	6.723805	0.812651	0.003503	1.756856
14	3.57851	1.070027	0.007395	1.765251
15	4.657033	0.838946	0.003771	1.761572

Table S1: The fitted coefficients of ruby's sideband

peak Num	Total Area	Gaussian Factor	FWHM	Peak Position
0.01969	0.084276	0.000105	1.80E-05	1.727664
0.016184	0.16074	0.000907	0.00032	1.732788
0.075511	0.383008	0.000521	0.000246	1.737033
0.030633	0.217768	0.000241	6.35E-05	1.737838
0.082723	0.222482	0.000142	5.87E-05	1.739351
0.085682	0.322255	0.001549	0.000295	1.746523
0.038629	0.083108	0.000184	5.09E-05	1.741731
0.012734	0.031189	3.06E-05	9.99E-06	1.742481
0.02795	0.188559	0.000223	7.98E-05	1.744572
0.561392	0.722062	0.00097	0.000279	1.749358
0.013347	0.064727	0.000154	4.39E-05	1.758876
0.100551	0.501026	0.002009	0.000257	1.752803
0.038153	0.318702	0.000395	0.000158	1.756856
0.198192	0.660828	0.003799	0.001812	1.765251
0.073787	0.412422	0.000491	4.87E-05	1.761572

Table S2: The 1σ error of fitted coefficients of table S1

A genetic algorithm was utilized in the fitting of the Stokes sideband. A total of 60 variables, 4 variables or each peak with the peak position, area under peak, Gaussian factor, and the FWHM with a total of 15 peaks. The initial population range of the peak position was set by the 0.001 eV interval of the estimated peak position which was manually adjusted too. The area variables having a initial population range of $0 \sim 4$, the Gaussian factor a range of $0 \sim 1$ and the peak FWHM a range of $0 \sim 0.01$. The lower bound of nonzero was given to the area, FWHM, Gaussian factor (this had an upper bound of 1 too) and the initial population range was given as upper and lower bounds for the peak position.

The execution was utilized using a MATLAB 'ga' function from the optimization toolbox, and run in parallel using the Parallel computing toolbox. It took ~ 1 hour for a single fit. The 'ga' algorithm rapidly converged the fit, however fine tuning was still needed afterwards, and this was used using the 'fitnlm' nonlinear fit function of MATLAB. Note that it is near impossible to fit using only nonlinear fitting functions.

S3 R-lines Fitting Results

Each Voigt (pseudo-Voigt) peak fitted coefficients (or calculated values in some cases) and the 1σ error are shown in the tables below. For the values of $T < 80\text{K}$, the lorentzian width is neglected (not a value) in the pseudo-Voigt function and the FWHM is written in the Gaussian width instead.

S3.1 Pseudo Voigt Profile Fitting

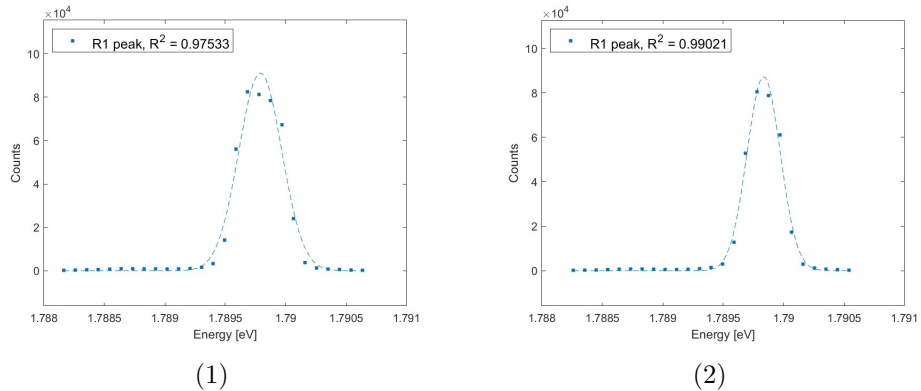


Figure S3: Result of Pseudo Voigt Profile of R_1 line with temperatrue of (1) 10K, (2) 20K.

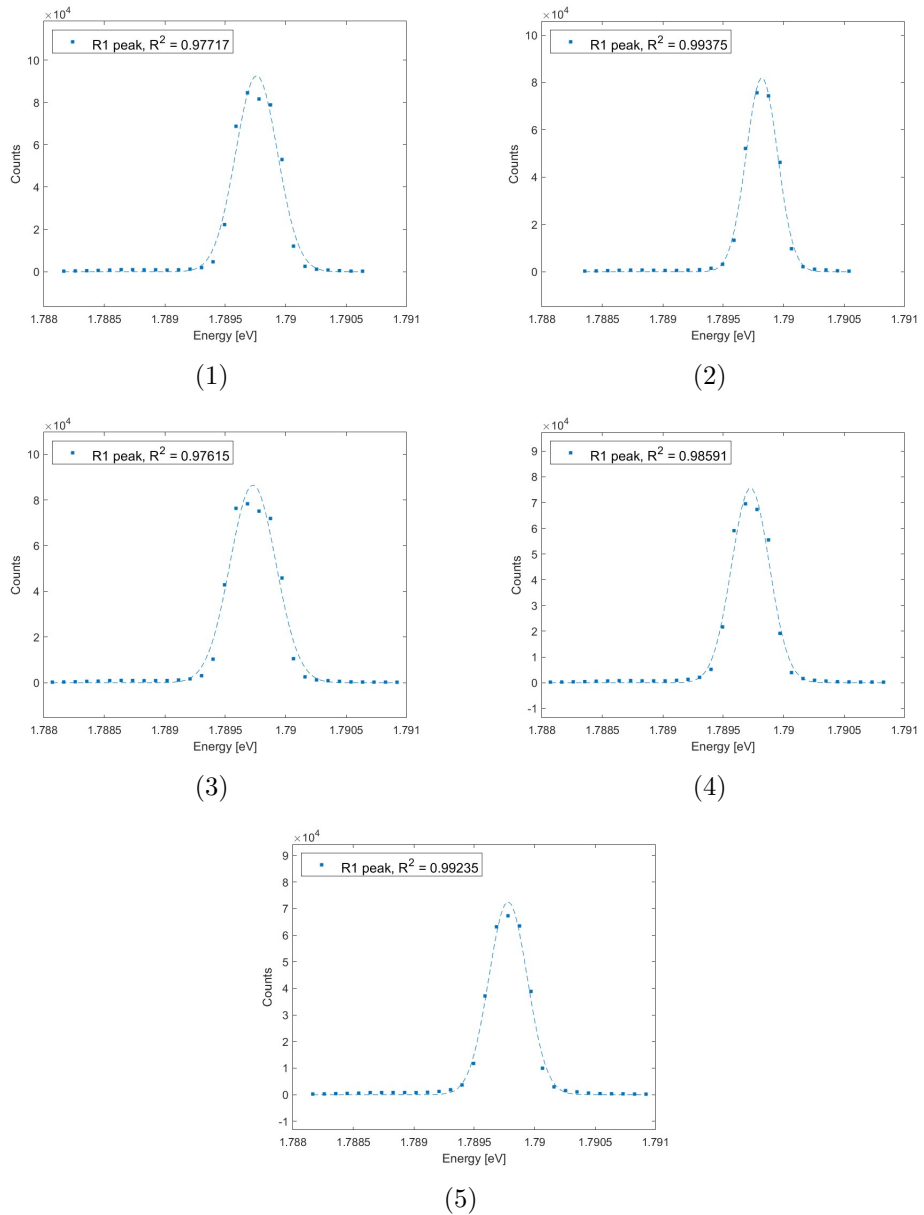


Figure S4: Result of Pseudo Voigt Profile of R_1 line with temperatrue of (1) 30K, (2) 40K, (3) 50K, (4) 60K, (5) 70K.

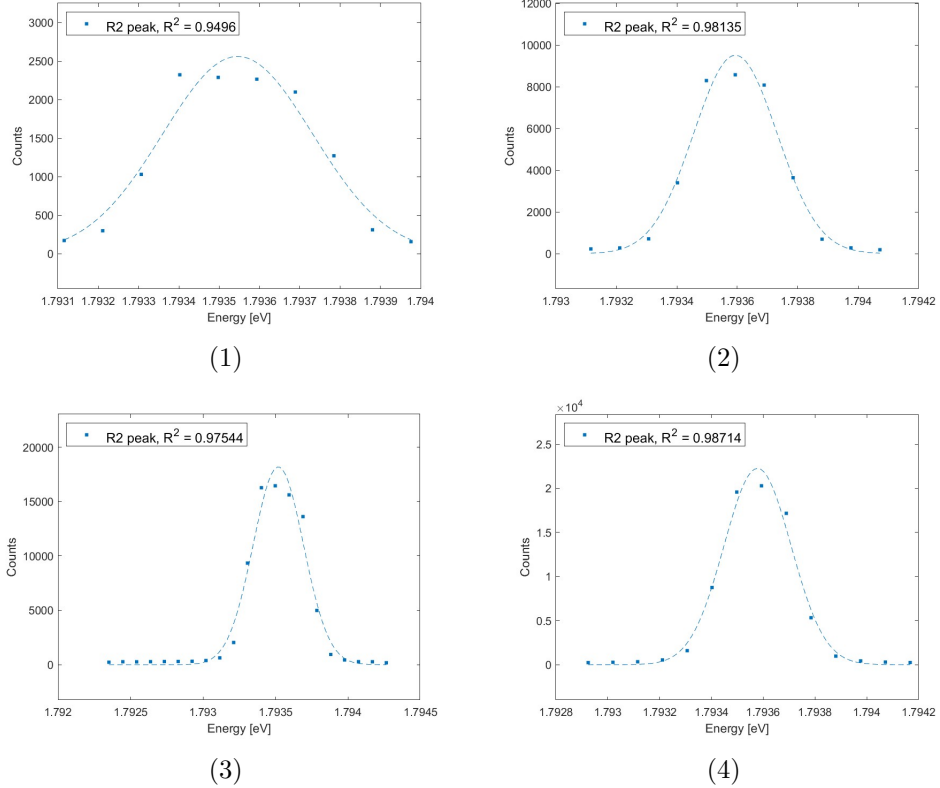


Figure S5: Result of Pseudo Voigt Profile of R_2 line with temperatrue of (1) 10K, (2) 20K, (3) 30K, (4) 40K

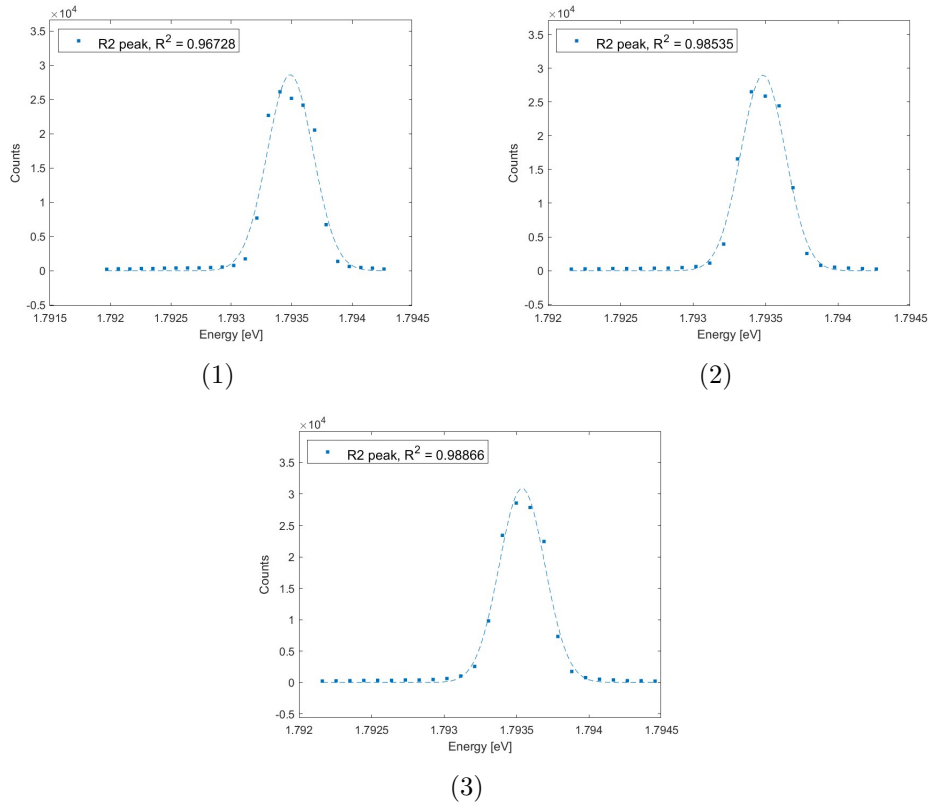


Figure S6: Result of Pseudo Voigt Profile of R_2 line with temperatrue of (1) 50K, (2) 60K, (3) 70K.

Temperature	peak height	1σ Error	peak position	1σ Error	Gaussian width	1σ Error	Lorentzian Width	1σ Error
10	91235.4153	7.85E-04	1.78978989	7.10E-06	4.39E-04	1.67E-05	0.00E+00	0
20	87416.7075	2.12E-05	1.78983402	3.67E-06	3.25E-04	8.63E-06	0.00E+00	0
30	92675.8996	0.00040014	1.78975919	6.69E-06	4.09E-04	1.57E-05	0.00E+00	0
40	82031.655	9.53E-03	1.78981943	2.83E-06	3.05E-04	6.67E-06	0.00E+00	0
50	86550.1767	0.00024439	1.78972929	6.96E-06	4.46E-04	1.64E-05	0.00E+00	0
60	75713.8224	3.80E-05	1.78972525	4.54E-06	3.62E-04	1.07E-05	0.00E+00	0
70	72624.2298	1.12E-06	1.78977795	3.38E-06	3.70E-04	7.97E-06	0.00E+00	0
80	86061.7384	5.54E-05	1.78968731	3.60E-06	1.87E-04	3.60E-06	2.14E-07	3.58E-09
90	79925.469	6.80E-06	1.78971237	2.69E-06	1.79E-04	2.69E-06	1.39E-06	1.80E-08
100	73467.0455	13525.8637	1.78971876	1.25E-06	1.34E-04	3.72E-06	7.43E-05	1.10E-05
110	89961.286	21185.9893	1.78961933	1.84E-06	1.71E-04	5.47E-06	8.47E-05	1.64E-05
120	63343.9836	8500.12039	1.78957204	1.55E-06	1.65E-04	4.75E-06	1.36E-04	1.33E-05
130	64456.0081	4001.34035	1.78955905	9.36E-07	1.41E-04	3.08E-06	2.10E-04	7.60E-06
140	72342.3759	4717.85005	1.78947703	1.12E-06	1.61E-04	3.68E-06	2.39E-04	9.11E-06
150	63285.9077	3460.29064	1.78940702	1.05E-06	1.62E-04	3.58E-06	2.89E-04	8.40E-06
160	57366.1669	2110.98605	1.78933476	7.39E-07	1.42E-04	2.75E-06	3.65E-04	5.62E-06
170	55441.4991	1895.22184	1.7892838	6.98E-07	1.39E-04	2.72E-06	4.08E-04	5.22E-06
180	54438.0958	1816.38176	1.78920547	7.33E-07	1.48E-04	2.88E-06	4.48E-04	5.47E-06
190	54405.3462	1984.25116	1.78912224	7.61E-07	1.57E-04	3.27E-06	4.88E-04	6.45E-06
200	52020.4589	1613.80008	1.7890754	7.03E-07	1.48E-04	2.96E-06	5.33E-04	5.13E-06
210	44897.728	1510.73658	1.78901861	6.85E-07	1.29E-04	3.19E-06	5.99E-04	4.74E-06
220	47496.7077	1909.62424	1.78892873	7.78E-07	1.38E-04	3.97E-06	6.44E-04	6.20E-06
230	39493.3232	1533.55373	1.78889525	8.07E-07	1.06E-04	3.53E-06	7.03E-04	3.96E-06
240	40994.0369	2009.51218	1.78875794	8.87E-07	0.00013417	5.12E-06	0.0007701	6.98E-06
250	26932.7599	2.37736225	1.78875943	1.21E-06	5.68E-05	3.57E-07	0.00084183	3.31E-06
260	31285.3671	10.8589316	1.7886422	1.11E-06	8.79E-05	4.56E-07	0.00091533	2.91E-06
270	29891.7618	395.773296	1.78853858	1.21E-06	0.00012159	1.76E-06	0.00096079	3.05E-06
280	30762.1532	1807.26208	1.78833545	1.18E-06	0.00016013	7.62E-06	0.00104747	9.62E-06

Table S3: Each pseudo-Voigt peak fitted coefficients (or calculated values in some cases) and the 1σ error of the R1-line

S3.2 Voigt Profile Fitting

Temperature	peak height	1σ Error	peak position	1σ Error	Gaussian width	1σ Error	Lorentzian Width	1σ Error
10	2562.56298	3.62E-05	1.79354598	1.35E-05	4.39E-04	3.21E-05	0.00E+00	0
20	9508.67912	4.18E-04	1.79359368	6.97E-06	3.25E-04	1.64E-05	0.00E+00	0
30	18185.2468	0.00042142	1.79351916	7.63E-06	4.09E-04	1.80E-05	0.00E+00	0
40	22263.9091	8.30E-05	1.79357811	5.10E-06	3.05E-04	1.20E-05	0.00E+00	0
50	28654.507	0.00158204	1.7934876	8.90E-06	4.46E-04	2.10E-05	0.00E+00	0
60	28967.5836	2.03E-04	1.79348299	5.12E-06	3.62E-04	1.20E-05	0.00E+00	0
70	30915.5928	1.04E-05	1.79353821	4.41E-06	3.70E-04	1.04E-05	0.00E+00	0
80	39247.2481	2.58E-03	1.79344395	7.85E-06	1.84E-04	7.88E-06	1.07E-07	3.99E-09
90	38777.8713	3.31E-04	1.79346981	5.51E-06	1.74E-04	5.51E-06	1.21E-07	3.32E-09
100	38012.7583	23400.7908	1.79347646	2.35E-06	1.37E-04	6.86E-06	3.91E-05	2.14E-05
110	47673.9272	91889.2339	1.79337647	3.39E-06	1.81E-04	9.73E-06	1.71E-05	3.17E-05
120	35050.8149	17253.878	1.7933302	2.70E-06	1.75E-04	7.93E-06	5.70E-05	2.46E-05
130	37432.5733	5171.44513	1.79331946	1.53E-06	1.48E-04	4.75E-06	1.34E-04	1.31E-05
140	42624.7966	6291.52247	1.79323883	1.80E-06	1.70E-04	5.55E-06	1.45E-04	1.55E-05
150	38126.7449	4295.92899	1.7931724	1.65E-06	1.71E-04	5.21E-06	1.85E-04	1.39E-05
160	35657.8907	2300.84215	1.7931041	1.11E-06	1.53E-04	3.71E-06	2.49E-04	8.96E-06
170	35207.6966	1967.38454	1.79305529	1.02E-06	1.47E-04	3.55E-06	2.87E-04	8.07E-06
180	34855.1509	1880.4412	1.79297878	1.06E-06	1.58E-04	3.69E-06	3.10E-04	8.41E-06
190	34830.781	1985.2664	1.79289718	1.10E-06	1.70E-04	4.08E-06	3.37E-04	9.65E-06
200	33739.6114	1563.67096	1.79285321	9.98E-07	1.62E-04	3.64E-06	3.72E-04	7.83E-06
210	29683.2685	1314.76136	1.79279982	9.46E-07	1.50E-04	3.65E-06	4.16E-04	7.27E-06
220	31206.1451	1540.31314	1.79271183	1.09E-06	1.73E-04	4.24E-06	4.28E-04	9.16E-06
230	26696.4556	1410.15508	1.79268078	1.08E-06	1.42E-04	4.61E-06	4.83E-04	8.47E-06
240	27691.5271	1392.82441	1.79254589	1.19E-06	0.00017939	4.86E-06	0.00050359	9.97E-06
250	18692.2792	1382.42064	1.79255097	1.55E-06	1.34E-04	6.88E-06	0.0005527	1.10E-05
260	21978.6961	1345.46556	1.79243837	1.40E-06	1.47E-04	6.27E-06	0.0006146	9.94E-06
270	21224.7476	1409.17003	1.79234051	1.52E-06	0.00016384	7.11E-06	0.00063985	1.24E-05
280	21989.725	1196.99944	1.79214764	1.46E-06	0.00019924	6.53E-06	0.00067759	1.23E-05

Table S4: Each Voigt peak fitted coefficients (or calculated values in some cases) and the 1σ error of the R2-line

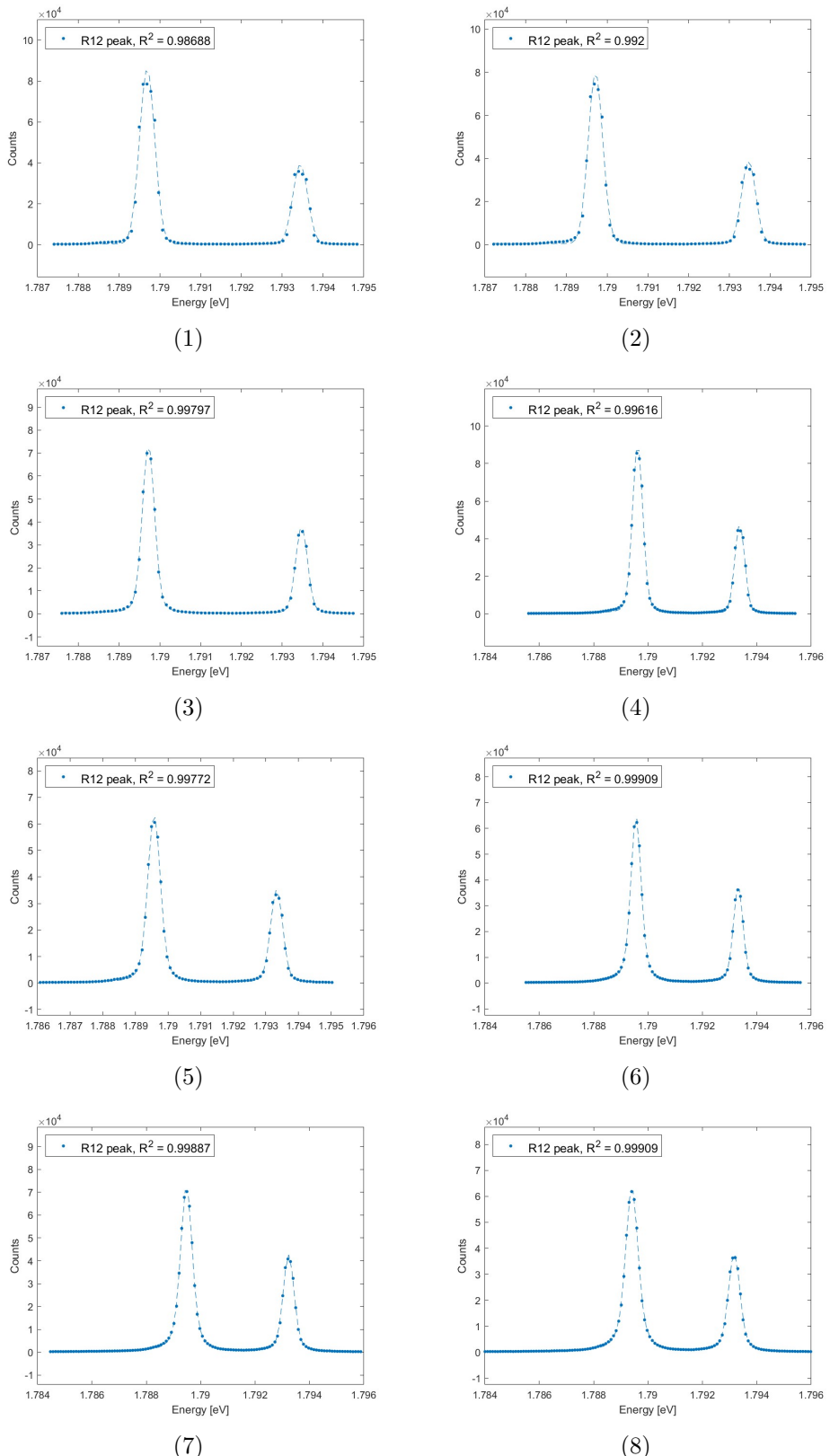


Figure S7: Result of Voigt Profile of R lines with temperattrue of (1) 80K, (2) 90K, (3) 100K, (4) 110K (5) 120K, (6) 130K, (7) 140K, (8) 150K.

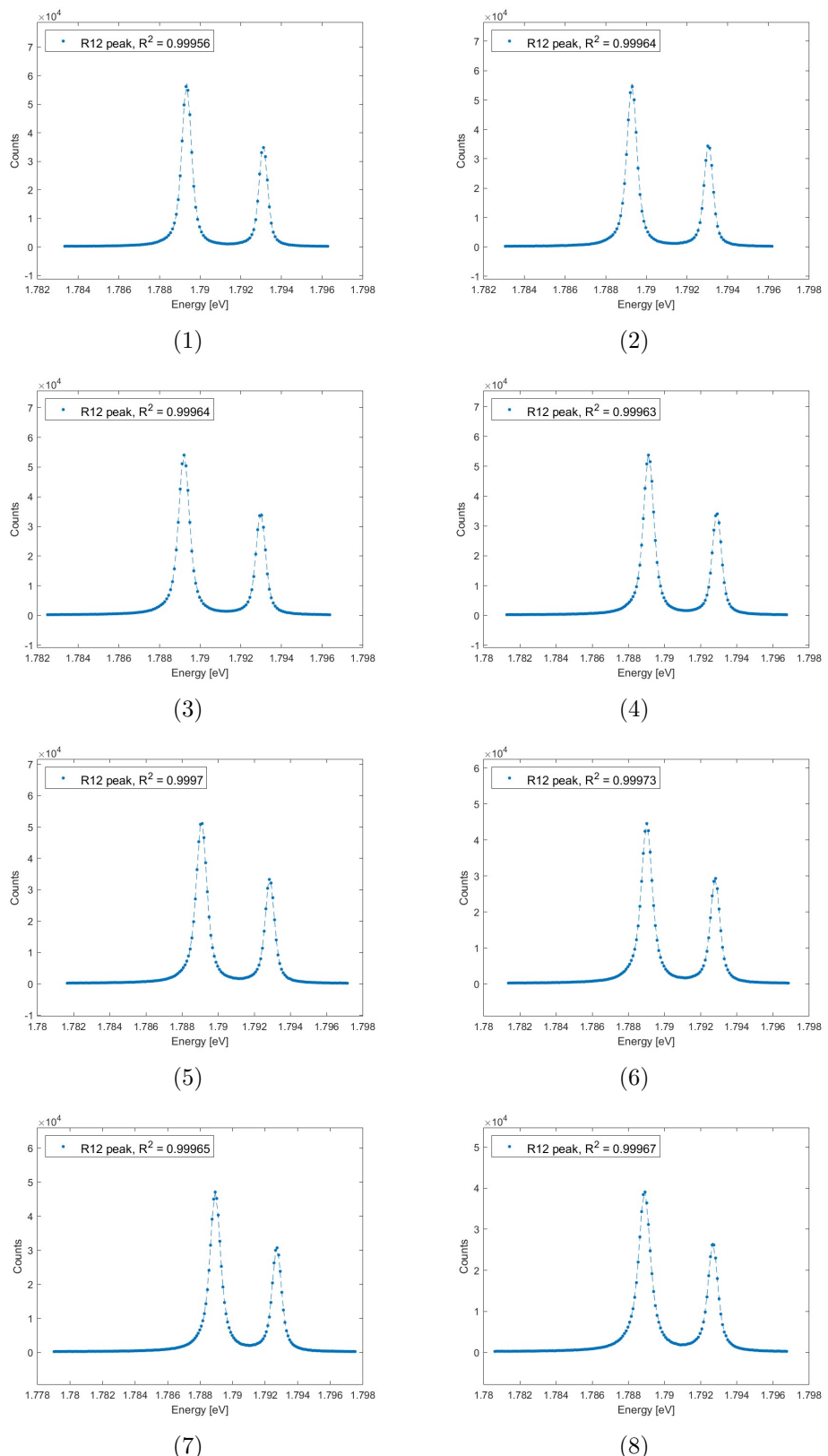


Figure S8: Result of Voigt Profile of R lines with temperatrue of (1) 160K, (2) 170K, (3) 180K, (4) 190K (5) 200K, (6) 210K, (7) 220K, (8) 230K.

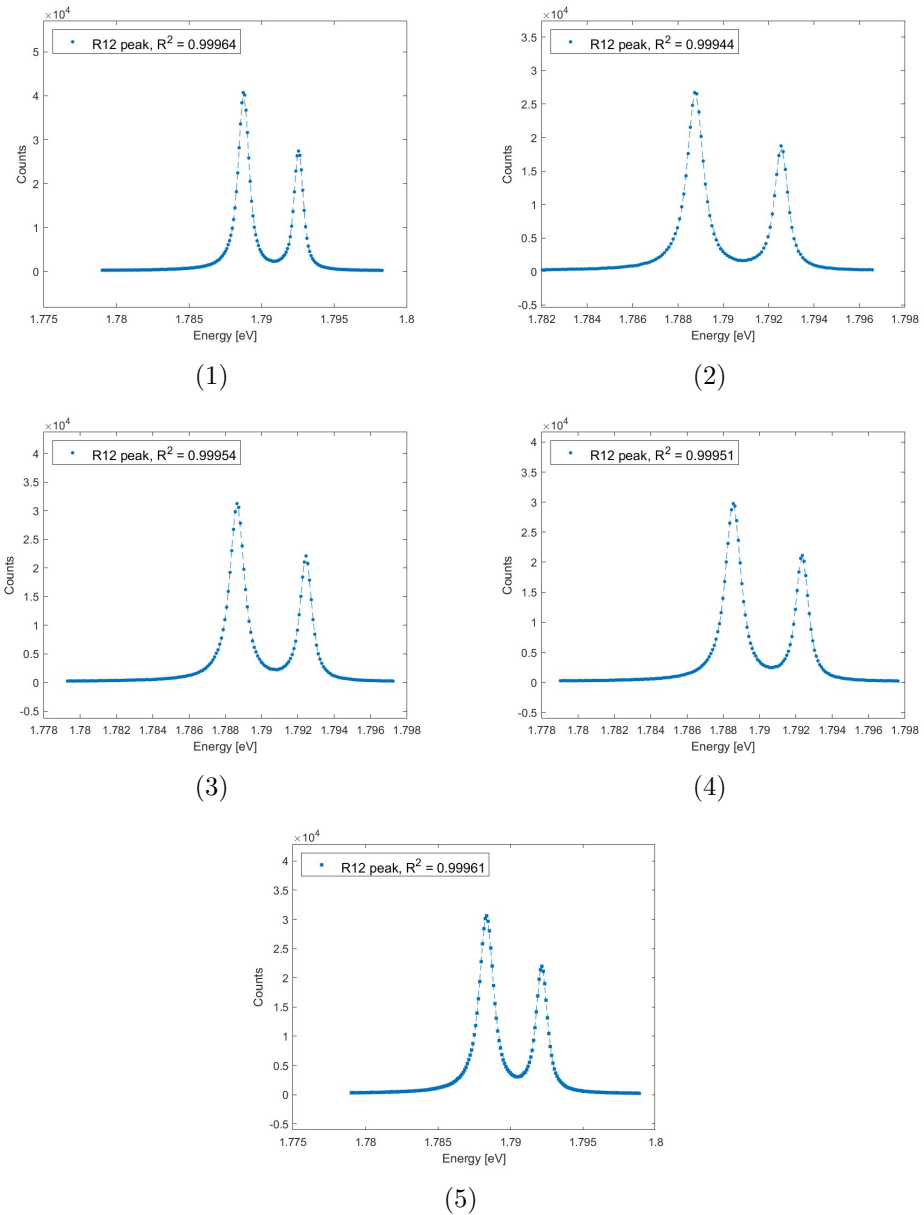


Figure S9: Result of Voigt Profile of R lines with temperatrue of (1) 240K, (2) 250K, (3) 260K, (4) 270K (5) 280K

S4 N_1 line

S4.1 Fitting Result

Each Gaussian peak fitted coefficients and the 1σ error are shown in the table and figures below.

Temperature	scale factor	1σ Error	Gaussian σ	1σ Error	peak position	1σ Error	peak height	1σ Error	R^2
10	0.44322795	0.03035791	0.00017112	1.36E-05	1.77E+00	1.35E-05	1.03E+03	70.7770714	1.36E-05
20	0.31712399	0.0135667	0.0001334	6.60E-06	1.77E+00	6.60E-06	9.48E+02	40.5711537	6.60E-06
30	0.39973737	0.02670094	0.00016452	1.27E-05	1.77E+00	1.27E-05	9.69E+02	64.7449457	1.27E-05
40	0.25635322	0.01142445	0.00012551	6.46E-06	1.77E+00	6.47E-06	8.15E+02	36.312229	6.46E-06
50	0.3602036	0.02314996	0.00018067	1.36E-05	1.77E+00	1.33E-05	7.95E+02	51.1180057	1.36E-05
60	0.22862535	0.01261852	0.00014938	9.53E-06	1.77E+00	9.53E-06	6.11E+02	33.699311	9.53E-06
70	0.19721025	0.01096368	0.00014789	9.51E-06	1.77E+00	9.50E-06	5.32E+02	29.5754261	9.51E-06
80	0.24508623	0.01869397	0.00017819	1.58E-05	1.77E+00	1.56E-05	5.49E+02	41.8537823	1.58E-05
90	0.18436131	0.00800391	0.00016675	8.37E-06	1.77E+00	8.36E-06	4.41E+02	19.1493616	8.37E-06
100	0.11463002	0.00273271	0.00013138	3.62E-06	1.77E+00	3.62E-06	3.48E+02	8.29774254	3.62E-06
110	0.15916366	0.0062572	0.00016142	7.34E-06	1.77E+00	7.33E-06	3.93E+02	15.4645398	7.34E-06
120	0.11894667	0.00656473	0.00016808	1.07E-05	1.77E+00	1.07E-05	2.82E+02	15.5812482	1.07E-05
130	0.10549998	0.00358324	0.00017112	6.72E-06	1.77E+00	6.71E-06	2.46E+02	8.35398802	6.72E-06
140	0.11746141	0.00716303	0.00019463	1.40E-05	1.77E+00	1.36E-05	2.41E+02	14.6820414	1.40E-05
150	0.0921148	0.0053344	0.00018553	1.25E-05	1.77E+00	1.24E-05	1.98E+02	11.4702031	1.25E-05
160	0.09166534	0.00387002	0.00020998	1.04E-05	1.77E+00	1.02E-05	1.74E+02	7.35257023	1.04E-05
170	0.08300235	0.00653382	0.00022032	2.04E-05	1.77E+00	1.98E-05	1.50E+02	11.8308353	2.04E-05
180	0.08184808	0.00447108	0.00025961	1.77E-05	1.77E+00	1.57E-05	1.26E+02	6.87059786	1.77E-05
190	0.07118962	0.00575152	0.00021789	2.09E-05	1.77E+00	2.01E-05	1.30E+02	10.5308537	2.09E-05
200	0.07358801	0.00600578	0.00025023	2.47E-05	1.77E+00	2.29E-05	1.17E+02	9.57494952	2.47E-05
210	0.06207544	0.00708907	0.00025182	3.49E-05	1.77E+00	3.22E-05	9.83E+01	11.2306342	3.49E-05
220	0.09113225	0.01735484	0.0003572	8.06E-05	1.77E+00	7.23E-05	1.02E+02	19.3831793	8.06E-05
230	0.03415363	0.00648106	0.00022655	5.19E-05	1.77E+00	4.85E-05	6.01E+01	11.4129512	5.19E-05

Table S5: The fitted Coefficients and their 1σ error. The R^2 of the fitting are also listed

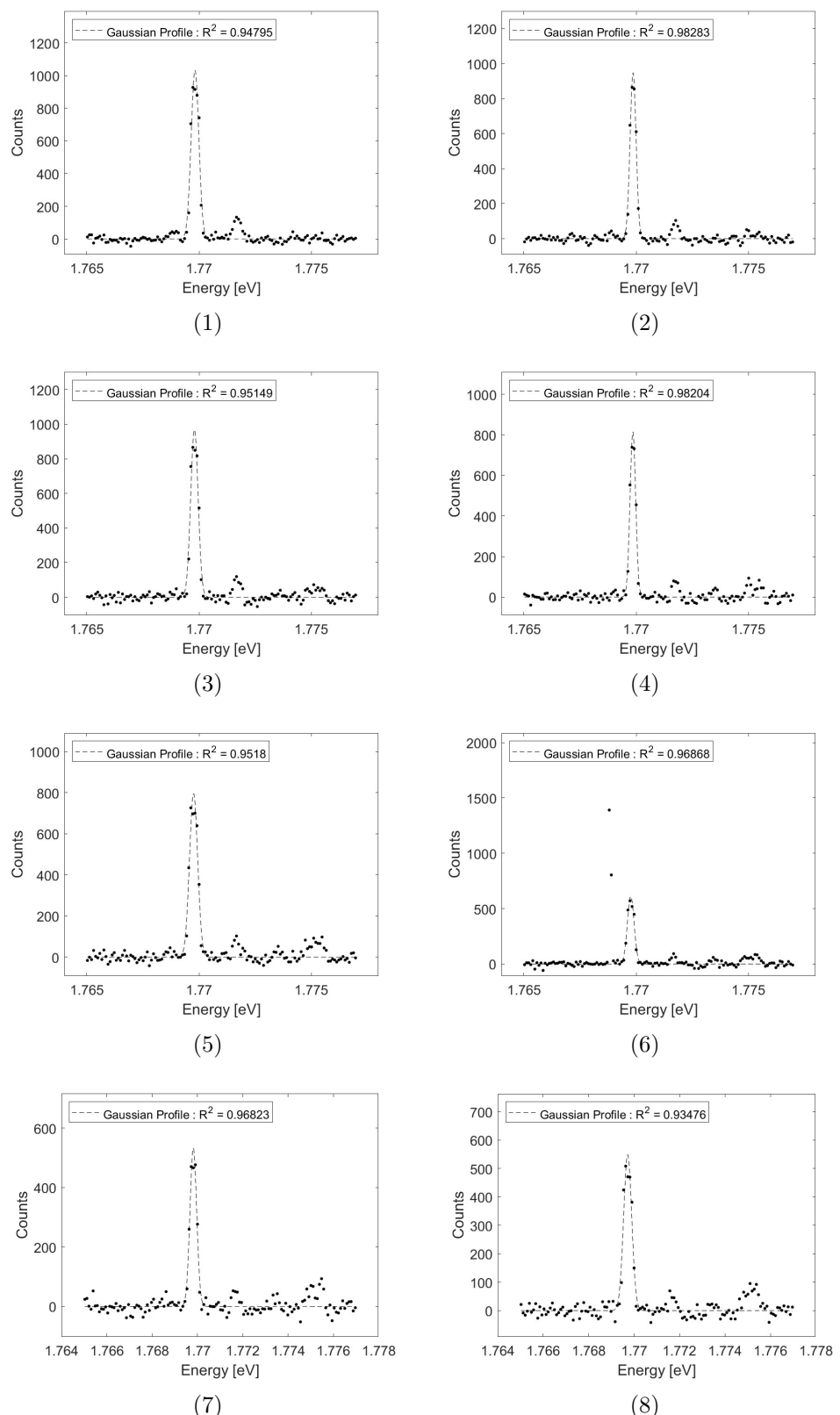


Figure S10: The result of Gaussian fit for N_1 line with temperature of (1) 10K, (2) 20K, (3) 30K, (4) 40K, (5) 50K, (6) 60K, (7) 70K, (8) 80K.

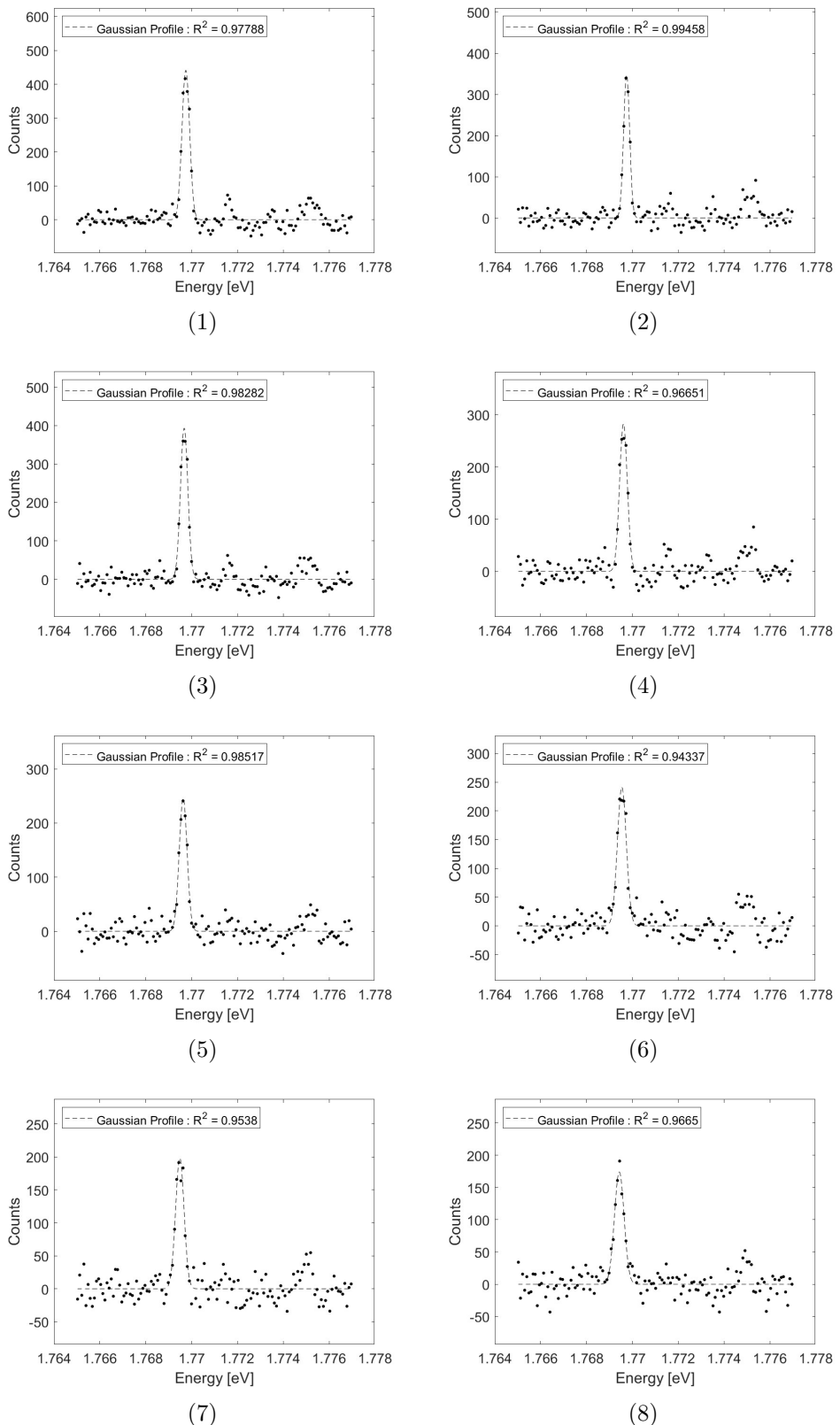


Figure S11: The result of Gaussian fit for N_1 line with temperature of (1) 90K, (2) 100K, (3) 110K, (4) 120K, (5) 130K, (6) 140K, (7) 150K, (8) 160K.

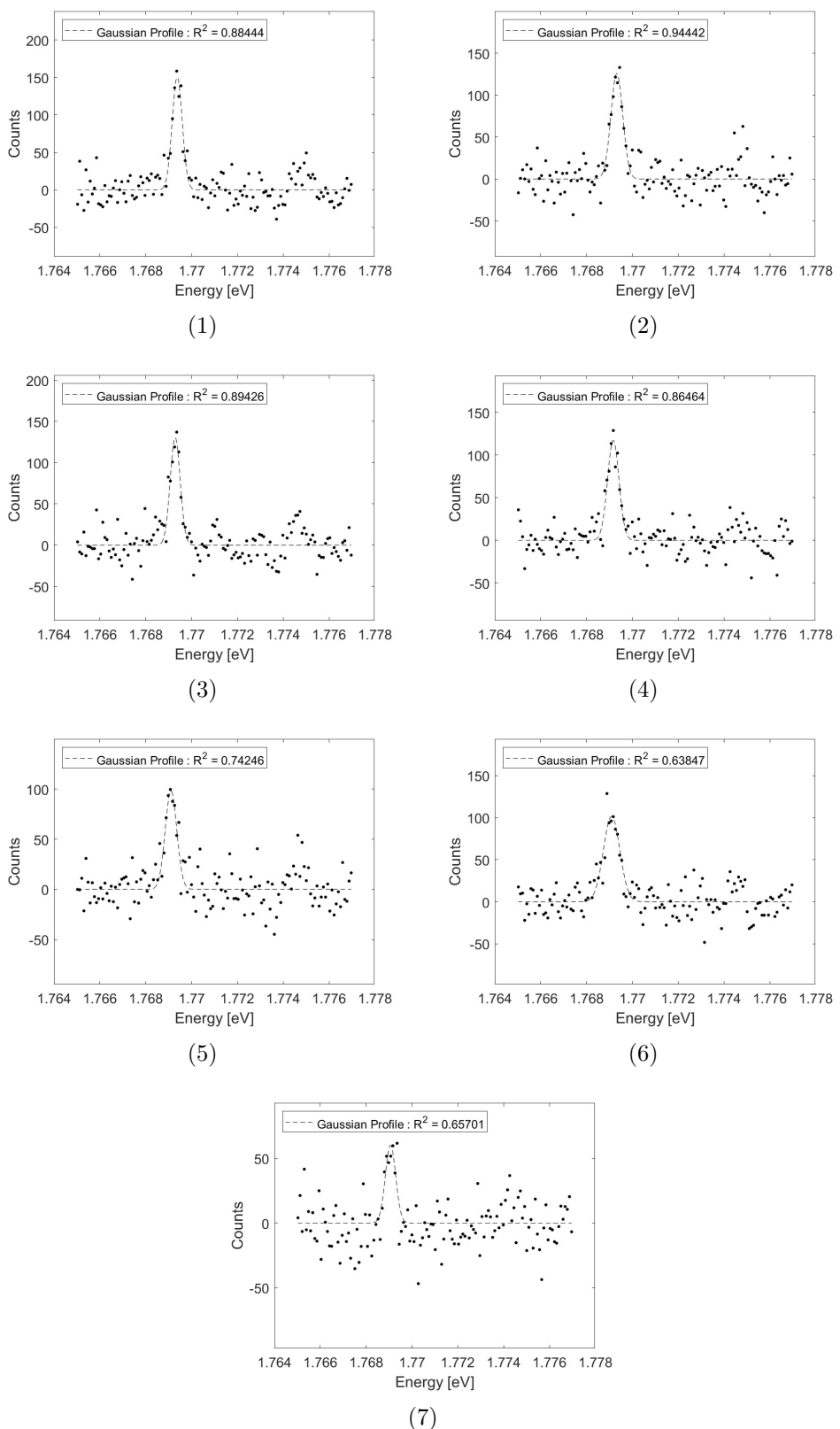


Figure S12: The result of Gaussian fit for N_1 line with temperature of (1) 170K, (2) 180K, (3) 190K, (4) 200K, (5) 210K, (6) 230K.

S4.2 Background Removal

The background 3rd order polynomial fit result are shown in the following table and figures.

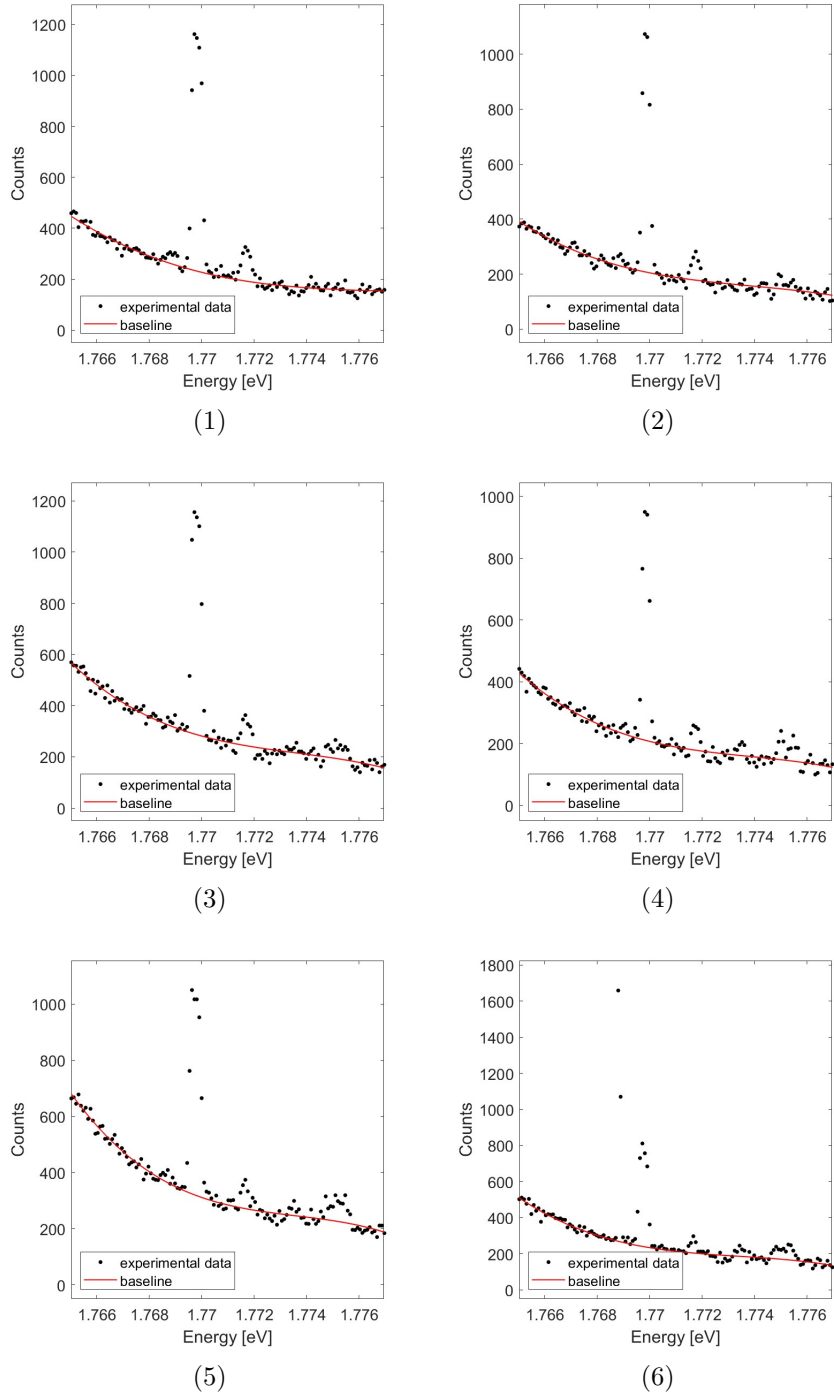


Figure S13: The result of extracting the baseline from the raw data with temperature of (1) 10K, (2) 20K, (3) 30K, (4) 40K, (5) 50K, (6) 60K.

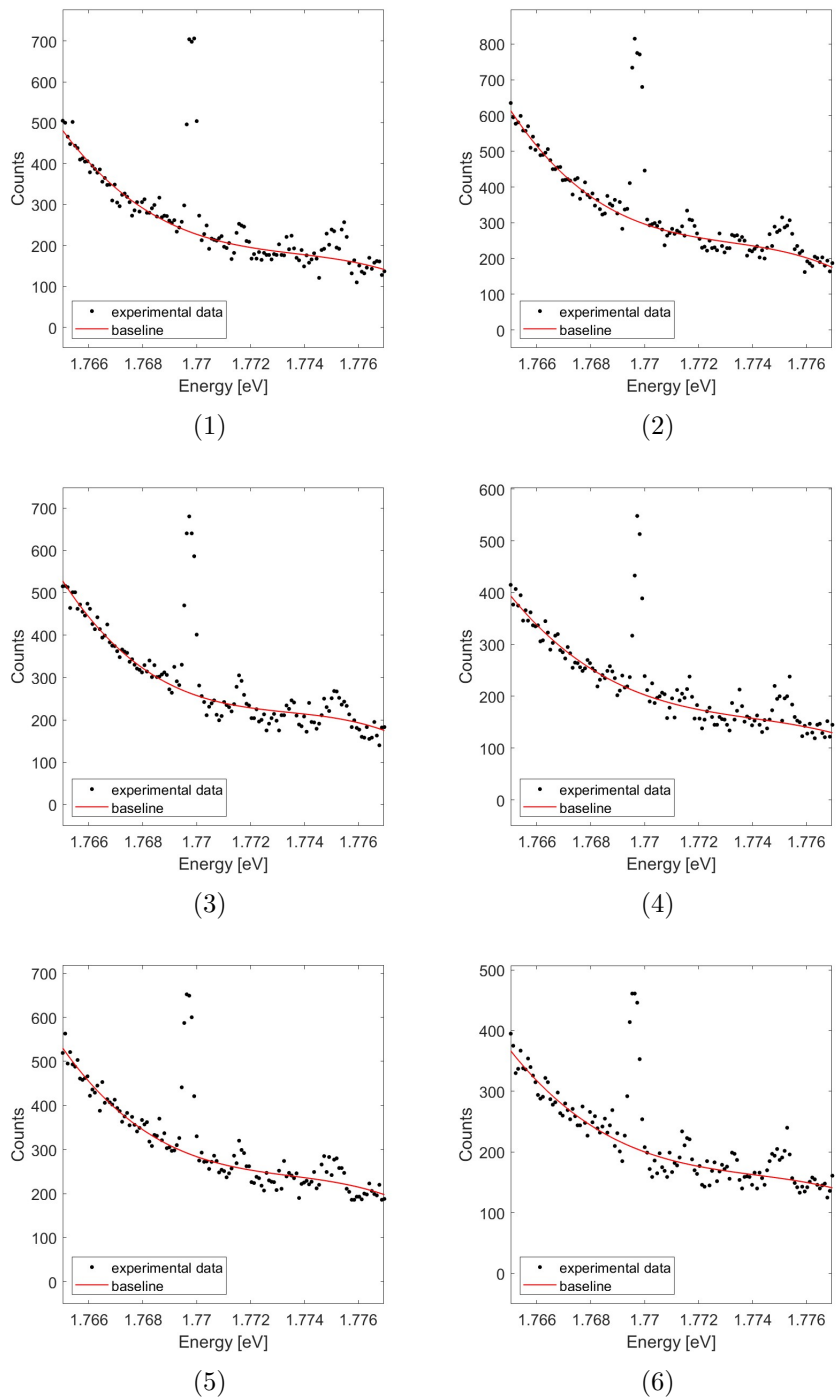


Figure S14: The result of extracting the baseline from the raw data with temperature of (1) 70K, (2) 80K, (3) 90K, (4) 100K, (5) 110K, (6) 120K.

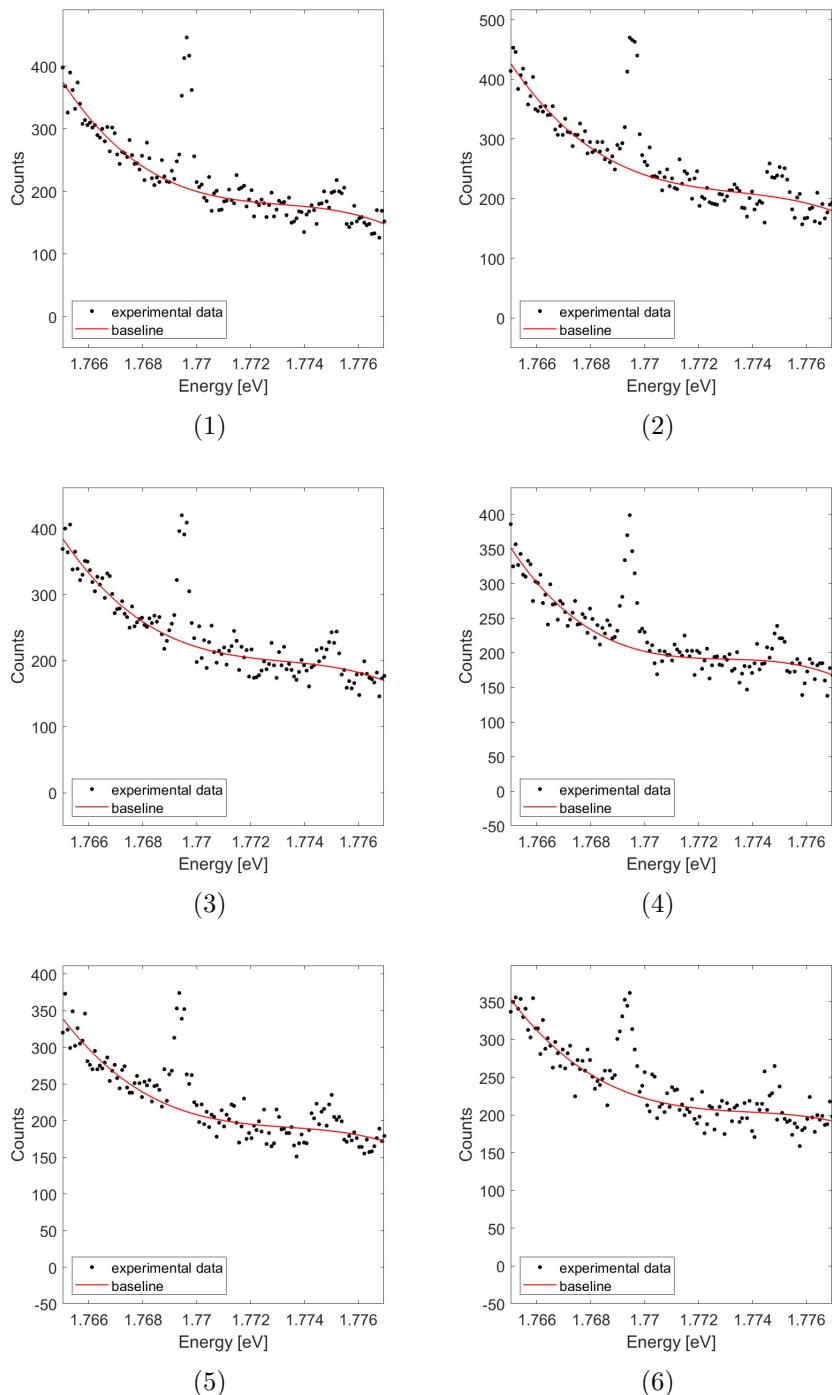


Figure S15: The result of extracting the baseline from the raw data with temperature of (1) 120K, (2) 140K, (3) 150K, (4) 160K, (5) 170K, (6) 180K.

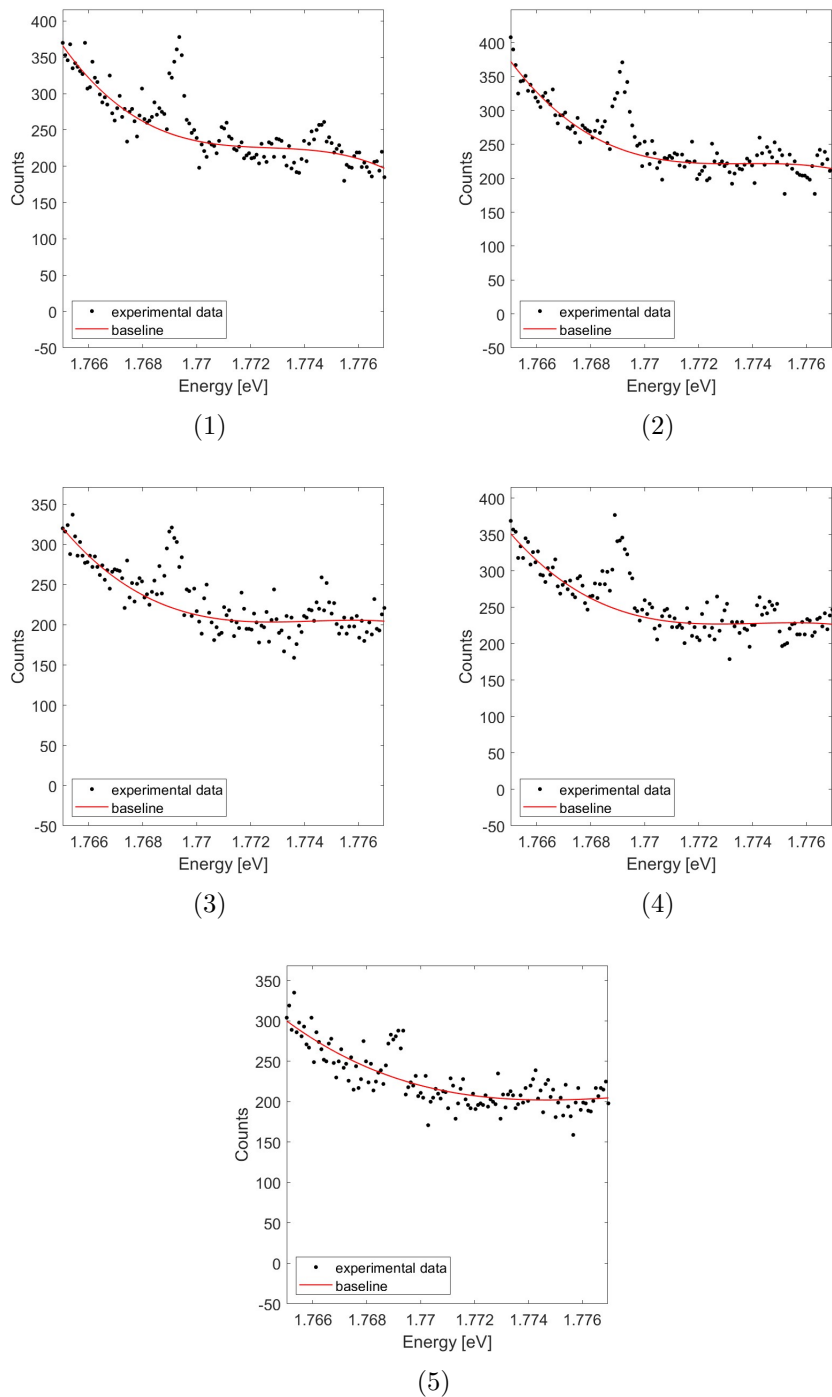


Figure S16: The result of extracting the baseline from the raw data with temperature of (1) 190K, (2) 200K, (3) 210K, (4) 220K, (5) 230K.

Temperature	a	1σ Error	b	1σ Error	c	1σ Error	d	1σ Error	R^2
10	-142091431	49932930.9	757610693	265307827	-1.35E+09	469884357	7.98E+08	277402157	9.70E-01
20	-223125775	53084537.9	1187401478	282048265	-2.11E+09	499524451	1.25E+09	294895399	9.54E-01
30	-368546120	58530342.7	1961010471	310984982	-3.48E+09	550776766	2.06E+09	325154414	9.78E-01
40	-282860956	53745863.4	1505262789	285559873	-2.67E+09	505739830	1.58E+09	298562308	9.68E-01
50	-536409764	64670579	2854135488	343606769	-5.06E+09	608547581	2.99E+09	359257000	9.81E-01
60	-417011122	76802532	2218612180	408124893	-3.93E+09	722916968	2.33E+09	426836488	9.68E-01
70	-356380065	61536551.9	1896327636	326963173	-3.36E+09	579085126	1.99E+09	341872263	9.55E-01
80	-516783885	60885056.4	2749042098	323512969	-4.87E+09	572994529	2.88E+09	338288358	9.74E-01
90	-432613221	67758258.8	2301600777	360023088	-4.08E+09	637641231	2.41E+09	376443978	9.53E-01
100	-229975338	53738496.4	1223967297	285535388	-2.17E+09	505722436	1.28E+09	298567377	9.48E-01
110	-364672443	66461374.2	1940252423	353137479	-3.44E+09	625455137	2.03E+09	369254988	9.43E-01
120	-202354724	53474051.8	1077000709	284133922	-1.91E+09	503246657	1.13E+09	297109493	9.34E-01
130	-314026450	53871450.9	1670428164	286241875	-2.96E+09	506973804	1.75E+09	299306209	9.16E-01
140	-292225631	62165854.4	1554717229	330314553	-2.76E+09	585034333	1.63E+09	345392451	9.13E-01
150	-281452345	56206466.4	1497218261	298649701	-2.65E+09	528951350	1.57E+09	312282191	9.04E-01
160	-302757602	52493379	1610360026	278920433	-2.86E+09	494007993	1.69E+09	291652339	8.81E-01
170	-216851777	52050790.6	1153687129	276568923	-2.05E+09	489843403	1.21E+09	289193804	8.74E-01
180	-195327889	53444728.8	1039426968	283975374	-1.84E+09	502961016	1.09E+09	296938023	8.64E-01
190	-286440060	51625583.4	1523322380	274309609	-2.70E+09	485841832	1.60E+09	286831356	8.61E-01
200	-234861488	47590768.5	1249718352	252870665	-2.22E+09	447870037	1.31E+09	264413356	8.88E-01
210	-158331089	52549892.5	842775897	279220315	-1.50E+09	494538390	8.84E+08	291965023	7.95E-01
220	-174481624	50317077	928667395	267355254	-1.65E+09	473521661	9.74E+08	279555977	8.31E-01
230	-46164923.4	52861538.3	246388172	280852288	-4.38E+08	497386534	2.60E+08	293621577	6.77E-01

Table S6: The table for coefficients of 3rd polynomial fitting of $y = ax^3 + bx^2 + cx + d$ with 1σ error and R^2 value.

S5 Dopping Estimation

S5.1 Fitting the Intensity Ratio of R-line & N-line

Coefficient	a	b	c	d
fitted value	-1.18E-07	7.12E-05	-0.01514	1.260768
1σ	1.30E-08	4.75E-06	0.000496	0.014047

Table S7: The coefficients 3rd order polynomial whose form is $ax^3 + bx^2 + cx + d$. The fitting is conducted by using the intensity ratio.

S5.2 Fitting the Relative Intensity According to the Concentration of Chromium

Note that the data that is used for the fitting is produced by [1].

Coefficient	a	b
fitted value	-1.18E-07	7.12E-05
1σ	0.050290977	0.053854

Table S8: The result of linear regression conducted to estimate the concentration of chromium in ruby from the relative intensity between R-line and N-line with the form of $y = ax + b$.

References

- [1] A. Monteil and E. Duval. Energy transfer in ruby. *Journal of luminescence*, 18:793–796, 1979.